

# Chapter 3

## Analytical derivation of localized approximate solution in the *twist-opening* model

### 3.1 Looking for an extension of the PB breathers

We have discussed in section 2.2.3 the possible biological meaning of the breather distortions that have been obtained in the PB model. We will now deal with the problem of determining if these approximate solution can be extended to the case of the helicoidal model. In other words, the question is to know whether a more accurate description of the helical geometry is still able to sustain essentially the same dynamical solutions of the PB model. We will find more complex localized solutions which present an angular distortion besides the radial one. The study of these solutions will shed light on the necessary structure of an oscillating opening of the double helix structure. The found solutions should be considered as the new dynamical objects involved in the studies of energy localization in DNA dynamical behavior.

Looking for localized solutions of the twist-opening equations of motion is difficult because we deal with a vectorial (two-component) field: the Multiple Scale Expansion (MSE) technique cannot be applied as it stands to this case. We show hereafter how to find in a general way small amplitude envelope soliton solutions in vectorial lattice problems. We will introduce in fact [17] an operator formalism that gives the MSE equations, up to the NLS one, from a perturbative expansion of the dispersion relations.

In this chapter, we give an interpretation of the underlying mathematics for the (scalar) MSE technique, pointing out why it fails in the case of vectorial fields. We then introduce the new formalism for *generic Klein-Gordon vectorial lattices*. It corresponds to a systematic reformulation of the MSE technique: an extension of the MSE approach to the multi-component case can become

extremely cumbersome, or even intractable for systems with many degrees of freedom. Our approach is formulated in a way that allows the treatment of complex systems and can eventually be programmed in symbolic languages to provide a fully automatic method. It is an important result, because it allows to apply the technique in complex cases, and with a reduced effort.

We have used this new approach to derive the envelope soliton solution in our helicoidal DNA model [16]. This will be presented in the last part of the chapter. The derivation of the new technique and its application to the model are quite complex. For this reason, the chapter is conceived as a more mathematical part, and we will keep the most of our biological reference themes apart from it.

Even in Section 3.3, where we apply the expansion operators to the twist-opening DNA model, we will discuss the result in the generic case. Only in section 3.4 we will come back to the biological implications. Starting from that section we will discuss which solutions exist with our parameter choice, and which are the interesting solutions in the context of our transcription initiation studies.

## 3.2 Multiple scale technique for multicomponent lattices

### 3.2.1 The Multiple Scale Expansion technique

We have already presented the standard MSE [37] in Section 2.2.2. It amounts to expanding the equations of motion on different time and space scales looking for wave-packet like solutions: such a solution is in fact characterized by an internal fast oscillation, that specifies the faster space and time scales, modulated by an envelope function that can be described on slower scales.

The assumption of the *wave-packet* structure is the true central point of the expansion, and the whole calculation could be presented in a more natural and rigorous way by keeping this in mind. A wave-packet is a superposition of plane waves whose frequencies and wave vectors lie in a narrow band, and it can be conveniently described by a plane wave with amplitude that varies slowly in space and time. By considering at the same time the two descriptions that one gets in the real space  $(x, t)$  and in its Fourier transformed space  $(q, \omega)$ , we can then identify the underlying fast oscillation with a central mode  $q_0$  of the linearized system; the slowness of the modulating function corresponds, in turn, to the narrowness of the wave number band. Starting from these considerations, the various steps of the standard MSE can be described as follows: increasing progressively the time and space scales one determines in a first step the *carrier wave* as a phonon mode of the linearized system, then deduces the partial differential equation that identifies the envelope velocity with the wave-packet *group velocity*, and, finally, derives the Non Linear Schrödinger (NLS) equation for the envelope, whose diffusion coefficient is in fact the wave-packet *group velocity dispersion*. The method,

used in optics, of expanding the dispersion relations with respect to one wave number and then to build at each order of this expansion an operator that acts on the envelope function is, in fact, analogous [56]. The non linearity coefficient in the NLS is obtained by including in an appropriate way the non linear terms deriving from the equations of motion.

MSE has been successfully applied to various non linear systems with scalar fields and the corresponding method adopted in optics has permitted the study of optical fiber properties. In this latter case, one deals with electric field components never coupled at the linear order of the Maxwell equations, so that the problem can always be reduced to a the case of a scalar field. However, many non linear models involve vectorial fields with coupled components at the linear order that give rise to dispersion relations with more than one branch: classical examples are given by multi-atomic lattices, or by lattices in which the mass in each site can move in a multidimensional space, as in our case.

While in the case of systems with only one degree of freedom per site the linearized problem is solved simply by finding a scalar dispersion relation that gives the frequency as a function of the vector number, in the case of vectorial fields the linear part corresponds to an eigen-value eigen-vector problem that is, *e.g.* in the case of two-component vectors, of the type  $\begin{pmatrix} a & b \\ c & d \end{pmatrix} \vec{V} = \omega^2 \vec{V}$ . This gives, at the same time, the frequencies described by the two branches  $\omega_+$  and  $\omega_-$  and the two eigen-vectors  $\vec{V}_+$  and  $\vec{V}_-$ : in order to look for small amplitude approximate solutions one has thus to perform a *perturbative expansion* instead of a simple Taylor expansion. Each of the two eigen-vectors specifies, in the Fourier transformed space, the relative amplitudes of the different components of the field: with respect to the scalar case, it is necessary to determine these relative amplitudes.

Besides the perturbative expansion, that treats the dispersive part of the equations of motion, one has to consider small amplitude solutions in order to introduce the *nonlinear terms* into the equations as successive corrections at increasing orders of accuracy. To combine the two effects of dispersion and non-linearity two parallel expansions with the common small parameter  $\epsilon$  have to be made; we show how they can be treated in an unique scheme to obtain the NLS equation for the envelope function in the general case of vectorial lattices with nonlinear on-site potentials and, possibly, non-Cartesian coordinate systems.

The general solution one finds with this technique has a main  $O(\epsilon)$  wave-packet contribution, proportional to  $\exp(q_0 t - \omega(q_0)x)$ , where  $q_0$  and  $\omega(q_0)$  are respectively a chosen central wave number and the corresponding frequency on one chosen branch. In addition there are some smaller  $O(\epsilon^2)$  terms corresponding to the eigen-vector perturbative correction and to the non oscillating (d.c.) and second harmonic contributions produced by the nonlinearity.

## 3.2.2 Wave-packet in linear vectorial lattices

### Equations of motion and wave-packet form of the solution

The NLS equation is obtained when a weak dispersion is balanced by a weak non-linearity. In order to characterize the dispersion, let us first restrict our attention to the linear part of the system of interest. We start with a one dimensional vectorial linear lattice model given by the equations of motion:

$$\frac{\partial^2 E(n, \nu, t)}{\partial t^2} = - \sum_{n', \nu'} J(n - n', \nu, \nu') E(n', \nu', t) \quad (3.1)$$

$n, n'$

where  $n, n'$  are the site indices,  $\nu, \nu'$  the indices that label the components of the the vectorial field  $E(n, \nu, t)$ , and  $J(n - n', \nu, \nu')$  are the force constants depending on  $n - n'$  for translationally invariant systems.

$\nu, \nu'$

$E(n, \nu, t)$

Looking for plane wave solutions of the form

$J(n - n', \nu, \nu')$

$$A \vec{V}_l(q) e^{i(qn - \omega_l(q)t)} + c.c. \quad (3.2)$$

$A$

where  $A$  is the wave amplitude and  $\vec{V}_l(q)$  is a normalized vector that specifies the ratio between the various field components the equation of motion is mapped to the following operator equation in the wave number space:

$\vec{V}_l(q)$

$$(\hat{J}(q) - \omega_l^2(q)) \vec{V}_l(q) = 0. \quad (3.3)$$

$\hat{J}(q)$

Here,  $\hat{J}(q)$  is the Fourier transform of the matrix  $\hat{J}(n - n')$ ; the index  $l$  runs from 1 to the number of components of the vectorial field  $E(n, \nu, t)$ . The eigenvalues functions  $\omega_l^2(q)$  that solve (3.3) give the branches of the dispersion relation; the normal modes  $\vec{V}_l(q)$  result then to be the orthonormal eigen-vectors of the matrix  $(\hat{J}(q) - \omega_l^2(q))$ .

$l$

$\omega_l^2(q)$

In order to investigate the dispersion, we now consider a wave-packet like solution, *i.e.* a superposition of plane waves with wave numbers in a small interval:

$$\vec{E}_l(n, t) = \int_{q_0 - \Delta q}^{q_0 + \Delta q} A(q) \vec{V}_l(q) e^{i(qn - \omega_l(q)t)} dq + c.c. \quad (3.4)$$

For each  $q$  contributing to the wave-packet the system (3.3) must be fulfilled. The weakly dispersive case is obtained by considering only small deviations of  $q$  with respect to the wave vector  $q_0$  corresponding to the center of the wave-packet. To indicate this deviation, the wave vector  $q$  is written  $q = q_0 + \epsilon q_1$ , where  $\epsilon \ll 1$ . Equation (3.3) is solved by a perturbative technique for all  $q_1$  in the integration range.

### Linear expansion of the system (3.3)

The operator  $\hat{J}(q_0 + q_1)$  can be expanded as

$$\hat{J}(q_0 + q_1) = \hat{J} + \epsilon \hat{J}' q_1 + \epsilon^2 \hat{J}'' q_1^2 / 2 + \dots, \quad (3.5)$$

$\hat{J}' = \hat{J}'(q_0)$ ,  $\hat{J}'' = \hat{J}''(q_0)$ , ... being the matrices whose components are the derivatives with respect to  $q$  of the  $\hat{J}(q)$  components, calculated at  $q = q_0$ . The quantities  $\epsilon \hat{J}'(q_0) q_1$ ,  $\epsilon^2 \hat{J}''(q_0) q_1^2 / 2$  are small perturbations with respect to unperturbed operator  $\hat{J}(q_0)$ , whose eigen-values are  $\omega_l^2 = \omega_l^2(q_0)$  and whose eigen-vectors  $\vec{V}_l = \vec{V}_l(q_0)$  constitute a complete base.

According to standard perturbation theory [57] we write the expansions of the eigen-vectors and eigen-values,

$$\vec{V}_l(q_0 + \epsilon q_1) = \vec{V}_l + \epsilon \vec{V}_l^{(1)} q_1 + \epsilon^2 \vec{V}_l^{(2)} q_1^2 / 2 + \dots \quad (3.6)$$

$$\omega_l(q_0 + \epsilon q_1) = \omega_l + \epsilon \omega_l^{(1)} q_1 + \epsilon^2 \omega_l^{(2)} q_1^2 / 2 + \dots \quad (3.7)$$

The corrections  $\vec{V}_l^{(1)}$ ,  $\vec{V}_l^{(2)}$ ,  $\omega_l^{(1)}$ ,  $\omega_l^{(2)}$  have to be determined. Equation (3.3) has to be solved at each order of the expansion:

at order  $\epsilon^0$  :

$$\hat{J} \vec{V}_l = \omega_l^2 \vec{V}_l \quad (3.8)$$

at order  $\epsilon^1$  :

$$q_1 (\hat{J} \vec{V}_l^{(1)} + \hat{J}' \vec{V}_l) = q_1 (2\omega_l \omega_l^{(1)} \vec{V}_l + \omega_l^2 \vec{V}_l^{(1)}) \quad (3.9)$$

at order  $\epsilon^2$  :

$$\begin{aligned} \frac{q_1^2}{2} (\hat{J}' \vec{V}_l^{(1)} + \frac{1}{2} \hat{J}'' \vec{V}_l + \frac{1}{2} \hat{J} \vec{V}_l^{(2)}) &= \\ &= \frac{q_1^2}{2} (\omega_l^{(1)2} \vec{V}_l + \omega_l \omega_l^{(2)} \vec{V}_l + 2\omega_l \omega_l^{(1)} \vec{V}_l^{(1)} + \frac{\omega_l^2}{2} \vec{V}_l^{(2)}) \end{aligned} \quad (3.10)$$

### Solution of (3.3) at different orders

At order  $\epsilon^0$ , one solves the unperturbed problem determining  $\vec{V}_l$  and  $\omega_l$ .

At order  $\epsilon$ , one determines  $\vec{V}_l^{(1)}$ ,  $\omega_l^{(1)}$ . Imposing to  $\vec{V}_l^{(1)}$  to be orthogonal to  $\vec{V}_l$  to guarantee the normalization of  $\vec{V}_l(q_0 + q_1)$ , and multiplying (3.9) by  $\vec{V}_m^*$  ( $m \neq l$ ), we obtain

$$\vec{V}_l^{(1)} = \sum_{m \neq l} \alpha_m \vec{V}_m \quad (3.11)$$

$$\alpha_m = \frac{\vec{V}_m^* \hat{J}' \vec{V}_l}{\omega_l^2 - \omega_m^2} \quad m \neq l; \quad (3.12)$$

multiplying by  $\vec{V}_l^*$  we get

$$\omega_l^{(1)} = \frac{\vec{V}_l^* \hat{J}' \vec{V}_l}{2\omega_l}. \quad (3.13)$$

At order  $\epsilon^2$ , one determines  $\omega_l^{(2)}$  by multiplying (3.10) by  $\vec{V}_l^*$ :

$$\omega_l^{(2)} = \frac{1}{\omega_l} \left( \vec{V}_l^* \frac{\hat{J}''}{2} \vec{V}_l - \omega_l^{(1)2} + \sum_{m \neq l} \frac{|\vec{V}_m^* \hat{J}' \vec{V}_l|^2}{\omega_l^2 - \omega_m^2} \right). \quad (3.14)$$

We are assuming that no degeneracy conditions for the relations (3.3) hold.

### Recollection of the various components in (3.4)

The phase of each component of (3.4) can be expanded around the central wave number  $q_0$ , up to second order in  $\epsilon q_1 = q - q_0$  using the values of  $\omega_l^{(1)}$  and  $\omega_l^{(2)}$  determined above. Under this form,  $\vec{E}_l(n, t)$  appears as a plane wave, henceforth called the carrier wave, with an amplitude  $\vec{F}(n, t)$  that depends on space and time and which corresponds to the integral of the following Equation (3.15):

$\vec{F}(n, t)$

$$\begin{aligned} \vec{E}_l(n, t) &= e^{i(q_0 n - \omega_l(q_0)t)} \vec{F}(n, t) = \epsilon e^{i(q_0 n - \omega_l(q_0)t)} \\ &\cdot \int_{-\Delta q/\epsilon}^{+\Delta q/\epsilon} \vec{V}_l(q_0 + \epsilon q_1) A(q_0 + \epsilon q_1) \exp \left\{ i\epsilon q_1 (n - \omega_l^{(1)}(q_0)t) - i\epsilon^2 \frac{q_1^2}{2} \omega_l^{(2)}(q_0)t \right\} dq_1 + c.c. \end{aligned} \quad (3.15)$$

The fact that  $\omega_l^{(1)}(q_0)$ ,  $\omega_l^{(2)}(q_0)$  obey to relations (3.13) and (3.14) ensures that this wave-packet is a solution of the original Equation (3.1), up to the order of the various expansions.

### Correspondences between the two Fourier transformed spaces and equations for $A(x_1, t_1, t_2)$

In order to extend the study to the nonlinear case it is useful to express these conditions under the form of an equation in the *space time coordinates* for the amplitude. Let us introduce the quantity

$$A(n, t) = \int_{-\Delta q/\epsilon}^{+\Delta q/\epsilon} A(q_0 + \epsilon q_1) \exp \left\{ i\epsilon q_1 (n - \omega_l^{(1)}(q_0)t) - i\epsilon^2 \frac{q_1^2}{2} \omega_l^{(2)}(q_0)t \right\} dq_1 + c.c. \quad (3.16)$$

$A(n, t)$

Equation (3.16) shows that  $A(n, t)$  depends slowly on space and time. In the spirit of the multiple scale expansion, it is natural to introduce the slow variables  $x_1 = \epsilon n$ ,  $t_1 = \epsilon t$  and  $t_2 = \epsilon^2 t$  so that  $A(n, t)$  can be written as

$x_1, t_1, t_2$

$$A(n, t) = A(x_1, t_1, t_2) = \int_{-\Delta q/\epsilon}^{+\Delta q/\epsilon} A(q_0 + \epsilon q_1) \exp \left\{ i q_1 (x_1 - \omega_l^{(1)}(q_0) t_1) - i \frac{q_1^2}{2} \omega_l^{(2)}(q_0) t_2 \right\} dq_1 + c.c. \quad (3.17)$$

or as

$$A(n, t) = A(s_1, t_2) = \int_{-\Delta q/\epsilon}^{+\Delta q/\epsilon} A(q_0 + \epsilon q_1) \exp \left\{ i q_1 s_1 - i \frac{q_1^2}{2} \omega_l^{(2)}(q_0) t_2 \right\} dq_1 + c.c. \quad (3.18)$$

with the introduction of the variable  $s_1$

$s_1$

$$s_1 = x_1 - \omega_l^{(1)}(q_0) t_1 \quad (3.19)$$

amounts to changing to the frame moving at the group velocity of the carrier wave.

From Equations (3.17) and (3.18) we derive directly the relation

$$(\partial A / \partial x_1) = (\partial A / \partial s_1) = i \langle q_1 \rangle, \quad (3.20)$$

where  $\langle \rangle$  indicates the average on the distribution  $A(q) \exp(i q_1 s_1 - i q_1^2 \omega_l^{(2)} t_2 / 2)$ . This relates to the wave-packet nature of the considered solution: each contribution of wave number  $q = q_0 + \epsilon q_1$  in (3.15) corresponds to a plane wave of type  $\exp(i q_1 s_1 - i q_1^2 \omega_l^{(2)} t_2 / 2)$  weighted, on the different field components, by the respective components of  $\vec{V}_l(q) A(q)$ .

Using (3.20) and the expansion (3.6) of  $V(q_0 + \epsilon q_1)$ , the amplitude  $\vec{F}$  of the wave can be expressed as a function of  $A(s_1, t_2)$  by the relation

$$\vec{F}(x_1, t_1, t_2) = \epsilon (\vec{V}_l - i \epsilon \vec{V}_l' \frac{\partial}{\partial x_1}) A(x_1, t_1, t_2). \quad (3.21)$$

We now directly derive the equations of motions of  $A$  as a function of the slow space-time variables by considering the derivatives of (3.17) and (3.18) and grouping the terms with equal order in  $q_1$ . This gives the two equations:

$$\left( \frac{\partial A}{\partial t_1} + \omega_l^{(1)} \frac{\partial A}{\partial x_1} \right) = 0 \quad (3.22)$$

and

$$i \frac{\partial A}{\partial t_2} + \frac{\omega_l^{(2)}}{2} \frac{\partial^2 A}{\partial s_1^2} = 0. \quad (3.23)$$

Thus  $\omega_l^{(1)}$  and  $\omega_l^{(2)}$  are the *group velocity* and the *group velocity dispersion* of the wave-packet and determine the peak velocity and the spread out of the envelope function. Equation (3.21) shows that  $\vec{V}_l'$  determines the first order correction to the direction of the vectorial field solution.

### 3.2.3 Non Linear Vectorial Lattice

We now consider the full equation of motion of a generic Klein-Gordon lattice, including nonlinear on-site potential terms. We also include nonlinear (on-site) terms depending on time derivatives, which could arise, in the case of non Cartesian coordinates systems, from the kinetic terms of the Lagrangian. The equations of motion can in this case be written in the following compact form:

$$\begin{aligned}
\frac{\partial^2 E(n, \nu, t)}{\partial t^2} = & - \sum_{n'} \sum_{\nu'} J(n - n', \nu, \nu') E(n', \nu', t) \\
& + \sum_{\substack{\nu'' \\ \nu' \leq \nu''}} \sum_{d=0}^2 \sum_{k=0}^d c_{d,k}^\nu(\nu', \nu'') E^{(k)}(n, \nu', t) E^{(d-k)}(n, \nu'', t) \\
& + \sum_{\substack{\nu''' \\ \nu'' \leq \nu''' \\ \nu' \leq \nu''}} \sum_{d=0}^2 \sum_{k=0}^d \sum_{j=0}^k C_{d,k,j}^\nu(\nu', \nu'', \nu''') E^{(j)}(n, \nu', t) E^{(k-j)}(n, \nu'', t) E^{(d-k)}(n, \nu''', t).
\end{aligned} \tag{3.24}$$

$E^{(j)}(n, \nu, t)$

$c_{d,k}^\nu$

$C_{d,k,j}^\nu$

$d$

$k, j$

$\nu, \nu'$

$\nu'', \nu'''$

Here  $E^{(j)}(n, \nu, t)$  indicates the  $j$ -th time derivative of  $E(n, \nu, t)$ , and  $c_{d,k}^\nu(\nu', \nu'')$ ,  $C_{d,k,j}^\nu(\nu', \nu'', \nu''')$  are the quadratic and cubic nonlinear terms numerical coefficients. Index  $d$  is the total time derivative order of each term. More precisely, the terms with  $d = 0$  are the simple quadratic and cubic terms in  $E$ , and correspond to the nonlinear force terms. The terms with  $d > 0$  derive (usually) from the kinetic energy in the case of non Cartesian coordinates, so that  $d \leq 2$ . The sums over  $k$  and  $j$  allow to group all the terms with a total order of derivative equal to  $d$  but with different orders of derivation for the two (three) field components comparing into  $c_{d,k}$  ( $C_{d,k,j}$ ). Index  $\nu$  corresponds to the number of the equation in the system (3.24),  $\nu'$ ,  $\nu''$  and  $\nu'''$  to the field components involved in the quadratic and cubic term considered, and represent the matrix indexes.

#### Second order corrections to the wave-packet solution arising from the non linearity

If we look for small amplitude wave-packet solution of the form (3.2), the quadratic terms in (3.24) give rise to second harmonic and constant (d.c.) terms. They arise from the two complex conjugate terms of (3.15), whose multiplication can be made so to have the same phase, or opposite phase. These additional contributions have to be included in the solution as smaller corrections:

$$\begin{aligned}
\vec{E}_l(n, t) = & \epsilon e^{i(q_0 n_0 - \omega_l(q_0) t_0)} (\vec{V}_l - i\epsilon \vec{V}_l' \frac{\partial}{\partial x_1}) A(x_1, t_1, t_2) \\
& + \epsilon^2 e^{2i(q_0 n_0 - \omega_l(q_0) t_0)} \vec{\gamma}_l A^2(x_1, t_1, t_2) + \epsilon^2 \vec{\mu}_l |A(x_1, t_1, t_2)|^2. \tag{3.25}
\end{aligned}$$



We are interested in situations where dispersion can balance nonlinearity, and therefore they must be measured by the *same scaling parameter*  $\epsilon$ . While the overall  $\epsilon$  factor was not important in the linear case, it must be explicitly included in the nonlinear case. This will shift of one order  $\epsilon$  all the equations derived in Section 3.2.2 for the linear case. Note that this implies that the nonlinear terms in  $E$  appear only at order  $\epsilon^2$  and  $\epsilon^3$ .

### Solution of the equation order by order

We solve the equation of motion (3.24) on the three wave-packet characteristic magnitude scales, as indicated, for the linear case, in Section 3.2.2.

At *order*  $\epsilon$  we get  $\omega_l(q_0)$ ,  $\vec{V}_l(q_0)$  from Equation (3.8).

At *order*  $\epsilon^2$ , and collecting all terms in  $\exp(q_0 t - \omega(q_0)x)$ , we get for the wave-packet term the system of Equations (3.9) for each  $q_1$ . After integration on the envelope distribution this gives rise in the anti-transform Fourier space to the equation

$$\left( 2\omega_l \vec{V}_l \frac{\partial}{\partial t_1} + (\hat{J} - \omega_l^2) \vec{V}_l^{(1)} \frac{\partial}{\partial x_1} + \hat{J}' \vec{V}_l \frac{\partial}{\partial x_1} \right) A(x_1, t_1, t_2) = 0. \quad (3.26)$$

In fact, from (3.17), a factor  $q_1$  in the Fourier space can be interpreted as  $-i\partial A/\partial x_1$  and a factor  $\omega_l' q_1$  can be interpreted as  $i\partial A/\partial t_1$ .

Multiplying (3.26) by  $V_m^* \forall m \neq l$  we obtain the components  $\alpha_m$  (3.12) of  $\vec{V}_l^{(1)}$  (3.11) on the base  $\{\vec{V}_m\}$  and multiplying (3.26) by  $V_l^*$  we obtain the Equation (3.22) with  $\omega_l^{(1)}$  defined by (3.13).

At the same order of expansion ( $\epsilon^2$ ) one determines the vectors  $\vec{\gamma}_l$ ,  $\vec{\mu}_l$  collecting the terms of corresponding order and phase in the equation of motion (3.24) in which the solution form (3.25) has been inserted. We obtain  $\vec{\gamma}_l$  from the  $\exp 2(q_0 t - \omega(q_0)x)$  terms. It is given by the system

$$(\hat{J}(2q_0) - 4\omega_l^2(q_0)) \vec{\gamma}_l = \sum_{d=0}^2 \sum_{k=0}^d \sum_{\substack{\nu'' \\ \nu' \leq \nu''}} \vec{c}_{d,k}(\nu', \nu'') (-i\omega_l)^d V_l(\nu') V_l(\nu'') \quad (3.27)$$

where  $\vec{c}_{d,k}(\nu', \nu'')$  represents the vector whose components are the matrices  $c_{d,k}^{\nu'}(\nu', \nu'')$ . Each derivative with respect to  $t_0$  gives a factor  $(-i\omega_l)$ .

$\vec{\mu}_l$  is obtained from the system that groups all the  $\exp(0)$  (d.c.) terms:

$$\begin{aligned} \hat{J}(0) \vec{\mu}_l = & \sum_{\substack{\nu'' \\ \nu' \leq \nu''}} \sum_{d=0}^2 \sum_{k=0}^d \vec{c}_{d,k}(\nu', \nu'') [(i\omega_l)^k (-i\omega_l)^{d-k} V_l^*(\nu') V_l(\nu'') \\ & + (-i\omega_l)^k (i\omega_l)^{d-k} V_l^*(\nu'') V_l(\nu')] . \end{aligned} \quad (3.28)$$

Note that if  $J(0)$  has some null columns then one has to add constant components at order  $\epsilon$  in (3.25). They enter in (3.28), and are then solved with the  $O(\epsilon^2)$  equations [16].

### The order $\epsilon^3$

At order  $\epsilon^3$ , from (3.24) and (3.25) and taking into account only the terms in  $\exp(i(q_0 n_0 - \omega_l(q_0)t_0))$ , we obtain the system of equations:

$$\begin{aligned}
& 2i\omega_l \vec{V}_l \frac{\partial}{\partial t_2} A(s_1, t_2) \\
& + \left( \left( \frac{1}{2} \hat{J}'' - \omega_l^{(1)2} \right) \vec{V}_l + (\hat{J}' - 2\omega_l \omega_l^{(1)}) \vec{V}_l^{(1)} + \left( \frac{1}{2} (\hat{J} - \omega_l^2) \vec{V}_l^{(2)} \right) \right) \frac{\partial^2}{\partial s_1^2} A(s_1, t_2) \\
& + \vec{Q} |A(s_1, t_2)|^2 A(s_1, t_2) = 0
\end{aligned} \tag{3.29}$$

$\vec{Q}$

where  $\vec{Q}$  denotes the vector whose components are obtained by collecting all the  $\epsilon^3$  terms arising from each equation of motion.  $\vec{V}_l^{(2)}$  is the second order correction to the chosen eigen-vector. It has not been calculated because it is inessential in order to find the desired envelope equations.

The first line of the Equation (3.29) corresponds to the third order expansion (3.10) of the linear operator Equation (3.3) applied to the wave-packet (terms in  $\exp(i(q_0 n_0 - \omega_l(q_0)t_0))$  in (3.25)), in the moving reference frame used in (3.23). We used again the properties of  $A$  that imply that a factor  $q_1$  leads to a term  $-i(\partial/\partial s_1)A(s_1, t_2)$ , a factor  $\omega_l^{(2)} q_1^2/2$  leads to  $i(\partial/\partial t_2)A(s_1, t_2)$ .

To write  $\vec{Q}$  we have to consider all the  $\exp(i(q_0 n_0 - \omega_l(q_0)t_0))$  terms arising from the multiplication of all the three contributions to the solution (3.25) and their derivatives; we must then calculate the respective coefficients, that will be written in terms of the matrices  $c_{d,k}^\nu(\nu', \nu'')$  and  $C_{d,k,j}^\nu(\nu', \nu'', \nu''')$  applied to the eigen-vectors and to the corrections  $\vec{\gamma}$ ,  $\vec{\mu}$ . The resulting  $\vec{Q}$  can be written as follows:

$$\begin{aligned}
\vec{Q} = & 2 \sum_{\substack{\nu'' \\ \nu' \leq \nu''}}^2 \sum_{d=0}^2 \vec{c}_{d,0}(\nu', \nu'') (-i\omega_l)^d \mu_l(\nu') V_l(\nu'') \\
& + \sum_{\substack{\nu'' \\ \nu' \leq \nu''}}^2 \sum_{d=0}^2 \sum_{k=0}^d \vec{c}_{d,k}(\nu', \nu'') \cdot \\
& \cdot \left( (i\omega_l)^k (-2i\omega_l)^{d-k} V_l^*(\nu') \gamma_l(\nu'') + (-2i\omega_l)^k (i\omega_l)^{d-k} V_l^*(\nu'') \gamma_l(\nu') \right) \\
& + \sum_{\substack{\nu''' \\ \nu'' \leq \nu''' \\ \nu' \leq \nu''}}^2 \sum_{d=0}^2 \sum_{k=0}^d \sum_{j=0}^k \vec{C}_{d,k,j}(\nu', \nu'', \nu''') \cdot
\end{aligned}$$

$$\begin{aligned}
& \cdot \left( (-i\omega_l)^j (-i\omega_l)^{k-j} (i\omega_l)^{d-k} V_l(\nu') V_l(\nu'') V_l^*(\nu''') \right. \\
& \quad + (-i\omega_l)^j (i\omega_l)^{k-j} (-i\omega_l)^{d-k} V_l(\nu') V_l^*(\nu'') V_l(\nu''') \\
& \quad \left. + (i\omega_l)^j (-i\omega_l)^{k-j} (-i\omega_l)^{d-k} V_l^*(\nu') V_l(\nu'') V_l(\nu''') \right) \quad (3.30)
\end{aligned}$$

We have introduced here also for the cubic coefficients a vector of matrices  $\vec{C}_{d,k,j}(\nu', \nu'', \nu''')$ .

The first three lines of the non linear coefficients vector  $\vec{Q}$  arise from the double product, in the nonlinear quadratic force terms in (3.24), between  $O(\epsilon)$  and  $O(\epsilon^2)$  components of (3.25); the last three lines arise from the nonlinear cubic force terms in (3.24) when considering just the  $O(\epsilon)$  terms in  $\vec{E}_l(n, t)$ .

### The NLS equation

Multiplying (3.29) by  $\vec{V}_l^*$ , and taking into account the orthogonality relations between different eigen-vectors (See Equation (3.11) and previous discussion), we finally obtain the *NLS equation*:

$$i \frac{\partial}{\partial t_2} A(s_1, t_2) + P \frac{\partial^2}{\partial s_1^2} A(s_1, t_2) + Q |A(s_1, t_2)|^2 A(s_1, t_2) = 0 \quad (3.31)$$

where the parameters  $P$  and  $Q$  are given by

$P, Q$

$$P = \omega_l^{(2)}/2 = \frac{1}{2\omega_l} \left( \vec{V}_l^* \hat{J}'' \vec{V}_l - \left( \frac{\vec{V}_l^* \hat{J}' \vec{V}_l}{2\omega_l} \right)^2 + \sum_{m \neq l} \frac{|\vec{V}_m^* \hat{J}' \vec{V}_l|^2}{\omega_l^2 - \omega_m^2} \right) \quad (3.32)$$

and

$$Q = \frac{\vec{V}_l^* \vec{Q}}{2\omega_l} \quad (3.33)$$

Equation (3.31) is the nonlinear version of (3.23) for the wave-packet; Equation (3.32) corresponds to (3.14). To the linear part it is now added the nonlinear part with coefficient  $Q$ .

If  $PQ > 0$  then the effect of the amplitude dependent non linear potential well in (3.31) balances the wave-packet group velocity dispersion giving rise to the stable *envelope soliton solution* [37] as already discussed in Section 2.2.2 and shown in Appendix A.

Following this approach it is straightforward to derive the NLS equation for every non linear vectorial lattice with on-site nonlinearities and with an arbitrary number of components. After having identified the nonlinear coefficients  $c_{d,k}^\nu(\nu', \nu'')$  and  $C_{d,k,j}^\nu(\nu', \nu'', \nu''')$  in the equation of motion (3.24), there are only

algebraic systems to solve: one has to solve the eigen-vectors  $V_l(q_0)$  and the eigen-values  $\omega_l(q_0)$  of the matrix  $\hat{J}(q_0)$ , then the systems (3.27) and (3.28) for  $\gamma_l$  and  $\mu_l$ , and to derive  $P$  from (3.32) and  $Q$  from (3.30) and (3.33).

From (3.31) one then obtains, if  $PQ \geq 0$ , the envelope function  $A(x_1, t_1, t_2)$  that, inserted into (3.25) together with the eigen-vector correction (3.11), (3.12), gives the complete  $O(\epsilon^2)$  solution we are looking for.

### 3.3 Analytical small localized solutions for the *twist-opening* model

#### 3.3.1 Application of the multicomponent MSE technique to the model

We will now apply the formalism described in Section 3.2 to the *twist-opening* model presented in the previous chapter. The field  $\vec{E}(n, t)$  correspond in our case to the two component field  $(y_n(t), \phi_n(t))$ . Being interested in small amplitude solutions we will refer to the approximate (rescaled) equations of motion (2.39), (2.40), reported here for clarity:

$$\begin{aligned} \ddot{y}_n &= \left(1 + \frac{y_n}{R_0}\right) \frac{1}{R_0} \dot{\phi}_n^2 - \left(y_n - \frac{3}{2}y_n^2 + \frac{7}{6}y_n^3\right) \\ &\quad - K_{yy}(y_{n+1} + y_{n-1} + 2y_n) - \frac{K_{y\phi}}{2}(\phi_{n+1} - \phi_{n-1}) \\ \ddot{\phi}_n &= -\frac{2}{R_0}\dot{y}_n\dot{\phi}_n - \frac{2}{R_0}y_n\ddot{\phi}_n - \frac{2}{R_0^2}y_n\dot{y}_n\dot{\phi}_n - \frac{1}{R_0^2}y_n^2\ddot{\phi}_n \\ &\quad + K_{\phi\phi}(\phi_{n+1} + \phi_{n-1} - 2\phi_n) + \frac{K_{y\phi}}{2}(y_{n+1} - y_{n-1}) \\ &\quad - G(\phi_{n+2} + \phi_{n-2} - 4\phi_{n+1} - 4\phi_{n-1} + 6\phi_n). \end{aligned}$$

From the linear part of these equations we immediately obtain the operator  $\hat{J}(q)$ , already introduced in Section 2.6.2, Equation (2.47):

$$\hat{J}(q) = \begin{pmatrix} a(q) & c(q) \\ c^*(q) & b(q) \end{pmatrix} \doteq \begin{pmatrix} 1 + 2K_{yy}(1 + \cos q) & iK_{y\phi} \sin q \\ -iK_{y\phi} \sin q & 2K_{\phi\phi}(1 - \cos q) \\ & + G(6 - 8 \cos q + 2 \cos 2q) \end{pmatrix}$$

and then the system giving the dispersion relations (3.3)

$$(\hat{J}(q) - \omega_{\pm}^2(q))\vec{V}_{\pm}(q) = 0.$$

We have used here the notation  $l = +, -$  for the index  $l$  that indicates the field component. This will make clearer the reference to the two dispersion branches, optical (+) and acoustic (-).

Corresponding to solve (3.3) to the order zero of expansion, we get eigenvalues (frequencies) and eigenvectors of system (3.3). They have been already found in Section 2.6.2, Equations (2.48) and (2.49):

$$\omega_{\pm}^2(q) = \frac{1}{2} \left( a + b \pm \sqrt{(a-b)^2 + 4|c|^2} \right)$$

$$\vec{V}^{\pm}(q) = \mathcal{N}_{\pm} \begin{pmatrix} 1 \\ (\omega_{\pm}^2 - a)/c \end{pmatrix}$$

### Linear expansion of the system: first order

We apply the perturbative expansion of the system (3.3) around one normal mode, as indicated in Section 3.2.2 by relations (3.5), (3.6) and (3.7). Just for clarity of notation, we choose here to indicate this mode as  $(q_0, \omega_+ = \omega_+(q_0))$ , referring to an excitation on the optical branch.

At order  $\epsilon$ , we obtain from (3.13) the wave-packet group velocity from the first order eigen-value correction  $\omega_+^{(1)}$ . Introducing for vectors the general notation  $\vec{V} = (V_1, V_2)$ , this gives:

$$\omega_+^{(1)} = \frac{\vec{V}^{+*} \hat{J}' \vec{V}^+}{2\omega_+} = \frac{1}{2\omega_+} (a' |V_1^+|^2 + c' V_1^{+*} V_2^+ + c'^* V_2^{+*} V_1^+ + b' |V_2^+|^2), \quad (3.34)$$

that represents the *group velocity* and defines the moving reference frame  $s_1 = x_1 - \omega_+^{(1)} t_1$  that follows the wave-packet. Primes indicate the derivatives of the  $J$  matrix elements with respect to  $q$  calculated at  $q_0$ .

We then obtain at the same order from (3.11) and (3.12) the correction to the eigen-vector  $\vec{V}^+$  that enters in the definition of the wave-packet amplitude  $F$  in (3.15) through Equation (3.21):

$$\vec{V}^{(1)} = \alpha \vec{V}^- \quad (3.35)$$

with

$$\alpha = \frac{\vec{V}^{-*} \hat{J}' \vec{V}^+}{\omega_+^2 - \omega_-^2} = \frac{a' V_1^{-*} V_1^+ + c' V_1^{-*} V_2^+ + c'^* V_2^{-*} V_1^+ + b' V_2^{-*} V_2^+}{\omega_+^2 - \omega_-^2}. \quad (3.36)$$

### Linear expansion of the system: second order

From the second order eigen-value correction (3.14) we obtain the *group velocity dispersion*  $\omega_+^{(2)}$ , that describes how the wave-packet spread out and that will enter

in the definition of the dispersion parameter  $P$  of the NLS equation. This gives:

$$\begin{aligned}\omega_+^{(2)} &= \frac{1}{\omega_+} (\vec{V}^{+*} \frac{\hat{J}''}{2} \vec{V}^+ - \omega_+^{(1)2} + \frac{|\vec{V}^{-*} \hat{J}' \vec{V}^+|^2}{\omega_+^2 - \omega_-^2}) \\ &= \frac{1}{\omega_+} (a'' |V_1^+|^2 + c'' V_1^{+*} V_2^+ + c''^* V_2^{+*} V_1^+ + b'' |V_2^+|^2 - \omega_+^{(1)2} + |\alpha|^2 (\omega_+^2 - \omega_-^2)).\end{aligned}\tag{3.37}$$

### Nonlinearity: form of the solution

The parameters  $\vec{V}^+$ ,  $\vec{V}^{(1)}$ ,  $\omega_+$ ,  $\omega_+^{(1)}$  and  $\omega_+^{(2)}$  are sufficient to write the dispersive part of the NLS equation for the envelope function, as explained in section 3.2.2. We now take into account the nonlinearity. We introduce the expansion parameter  $\epsilon$  for the solution in order to solve the equations at increasing order of accuracy, through the insertion of the nonlinear terms in a progressive way and the combination of this expansion with the expansion in multiple scales for the weak dispersive wave-packet. We introduce the variables  $x_1 = \epsilon x$ ,  $t_1 = \epsilon t$ ,  $t_2 = \epsilon^2 t$  for the slowly varying amplitudes. We look then for a solution of the form

$$\begin{aligned}\vec{E}(n) &= \epsilon e^{i(q_0 n_0 - \omega_+ t_0)} \left( \vec{V}^+ - i\epsilon \vec{V}^{(1)} \frac{\partial}{\partial x_1} \right) A(x_1, t_1, t_2) + \epsilon \vec{\sigma}(x_1, t_1, t_2) \\ &+ \epsilon^2 e^{2i(q_0 n_0 - \omega_+ t_0)} \vec{\gamma}(x_1, t_1, t_2) + \epsilon^2 \vec{\mu}(x_1, t_1, t_2)\end{aligned}\tag{3.38}$$

where the first term is the wave-packet, and the constant and second harmonic  $\epsilon^2$  terms are induced by the quadratic nonlinearity in the equation of motion, corresponding to Equation (3.38).

$\vec{\sigma}(x_1, t_1, t_2)$

The second  $O(\epsilon)$  term  $\vec{\sigma}(x_1, t_1, t_2)$  arises because the linear system (3.3) admits a constant solution with a non zero second component, corresponding to the null column of  $\hat{J}(0) = \begin{pmatrix} 1+4K_{yy} & 0 \\ 0 & 0 \end{pmatrix}$ . The calculation of this non oscillating solution has to be made together with that of the second order d.c. terms, as we will see.

We have at this point to determine the slowly varying amplitudes  $A(x_1, t_1, t_2)$ ,  $\vec{\sigma}(x_1, t_1, t_2)$ ,  $\vec{\gamma}(x_1, t_1, t_2)$ ,  $\vec{\mu}(x_1, t_1, t_2)$ .

### Second harmonic terms

From the equations of motion (2.39), (2.40) we easily calculate the nonlinearity matrices  $c_{d,k}^\nu$  and  $C_{d,k,j}^\nu$ : they are reported in Appendix B. Using the resulting  $c_{d,k}^\nu$ , we receive for the algebraic system (3.27) for the second harmonic terms:

$$(\hat{J}(2q_0) - 4\omega_+^2) \vec{\gamma} = \begin{pmatrix} \frac{3}{2} V_1^{+2} - \frac{\omega_+^2}{R_0} V_2^{+2} \\ \frac{4\omega_+^2}{R_0} V_1^+ V_2^+ \end{pmatrix} A^2.\tag{3.39}$$

With the introduction of a solution of the type

$$\vec{\gamma} = \vec{\gamma}_c A^2 \quad (3.40)$$

this reduces to a simple system for  $\vec{\gamma}_c$ , whose solution is given in Appendix C.

### Constant terms

For the constant terms we have to consider all the  $O(\epsilon^2)$  terms proportional to  $\exp(0)$  in the expansion of the system (3.3).

Because of the presence of the additional constant term  $\vec{\sigma}(x_1, t_1, t_2)$  at  $O(\epsilon)$ , this step does not correspond only to the system (3.28). We also have to apply the linear part of the system (3.24) to  $\vec{\sigma}$  and to consider its contribution to the  $\exp(0)$  terms order by order. At order  $\epsilon$  this gives simply  $\hat{J}(0)\vec{\sigma} = 0$ , so that we have to put, as anticipated,

$$\vec{\sigma} = (0, \sigma_2). \quad (3.41)$$

At order  $\epsilon^2$ , anyway, the expansion of the linear system applied to  $\vec{\sigma}$  gives a term  $-i\hat{J}'(0)\frac{\partial}{\partial x_1}\vec{\sigma}$ , to be added to (3.28). We have then

$$\hat{J}(0)\vec{\mu} - i\hat{J}'(0)\frac{\partial}{\partial x_1}\vec{\sigma} = \begin{pmatrix} 3|V_1^+|^2 + \frac{2\omega_+^2}{R_0}|V_2^+|^2 \\ 0 \end{pmatrix} |A|^2, \quad (3.42)$$

that gives a single equation,

$$a(0)\mu_1 - ic'(0)\frac{\partial}{\partial x_1}\sigma_2 = (3|V_1^+|^2 + \frac{2\omega_+^2}{R_0}|V_2^+|^2) |A|^2. \quad (3.43)$$

This equation does not suffice to determine the two unknowns  $\mu_1$  and  $\sigma_2$ . We have then to consider also the  $O(\epsilon^3)$  system of equations for the constant terms, that contains again a term in  $\vec{\sigma}$ <sup>1</sup>:

$$-i\hat{J}'(0)\frac{\partial}{\partial x_1}\vec{\mu} - \frac{\hat{J}''(0)}{2}\frac{\partial^2}{\partial x_1^2}\vec{\sigma} = \begin{pmatrix} \frac{2i\omega_+}{R_0}|V_2^+|^2(A^*\frac{\partial A}{\partial t_1} - \frac{\partial A^*}{\partial t_1}A) \\ \frac{2i\omega_+}{R_0}(V_2^{+*}V_1^+ - V_1^{+*}V_2^+)\frac{\partial}{\partial t_1}|A|^2 \end{pmatrix}. \quad (3.44)$$

The system (3.44) corresponds to the two following equations:

$$-ic'(0)\frac{\partial}{\partial x_1}\mu_2 = \frac{2i\omega_+}{R_0}|V_2^+|^2\left(A^*\frac{\partial A}{\partial t_1} - \frac{\partial A^*}{\partial t_1}A\right) \quad (3.45)$$

$$-ic'^*(0)\frac{\partial}{\partial x_1}\mu_1 - \frac{b''(0)}{2}\frac{\partial^2}{\partial x_1^2}\sigma_2 = \frac{2i\omega_+}{R_0}(V_2^{+*}V_1^+ - V_1^{+*}V_2^+)\frac{\partial}{\partial t_1}|A|^2. \quad (3.46)$$

---

<sup>1</sup>The r.h.s. of Equation (3.44) has been calculated directly from the equation of motion.

Equation (3.46) can be integrated using the wave-packet property (3.22),  $\partial A/\partial t_1 = -\omega_+^{(1)}\partial A/\partial x_1$ : we obtain then from (3.43), (3.46) the following system for  $\mu_1$  and  $\sigma_2$

$$\begin{pmatrix} a(0) & -ic'(0) \\ -ic'^*(0) & -\frac{b'(0)}{2} \end{pmatrix} \begin{pmatrix} \mu_1 \\ \partial\sigma_2/\partial x_1 \end{pmatrix} = \begin{pmatrix} 3|V_1^+|^2 + \frac{2\omega_+^2}{R_0}|V_2^+|^2 \\ \frac{-2i\omega_+\omega_+^{(1)}}{R_0}(V_2^{+*}V_1^+ - V_1^{+*}V_2^+) \end{pmatrix} |A|^2 \quad (3.47)$$

that gives

$$\mu_1 = \mu_{1c}|A|^2 \quad (3.48)$$

$$\sigma_2 = \sigma_{2c} \int |A|^2 dx_1. \quad (3.49)$$

Coefficients  $\mu_{1c}$  and  $\sigma_{2c}$  can be calculated algebraically and are reported in Appendix C.

Equation (3.45) gives  $\mu_2$  as function of the amplitude function. It can be explicitly solved only after having calculated the wave-packet amplitude, anyway we can anticipate that it will have the form

$$\mu_2 = \mu_{2c} \int |A|^2 dx_1 \quad (3.50)$$

with coefficient  $\mu_{2c}$  given in Appendix C.

We have then all the terms in (3.38) as functions of the amplitude  $A$ , that has now to be determined.

### Third order of expansion: the NLS equation

The nonlinear  $O(\epsilon^3)$  terms in  $\exp i(q_0 n_0 - \omega_+ t_0)$  in the equations of motion give rise to the nonlinearity that balances the group velocity dispersion of the wave-packet. We immediately obtain, from (3.31), the Non Linear Schrödinger equation for the envelope  $A$  expressed in a frame moving with velocity  $\omega_+^{(1)}$  (variables  $s_1 = x_1 - \omega_+^{(1)}t_1$  and  $t_2$ ):

$$iA_{t_2} + PA_{s_1 s_1} + Q|A|^2 A = 0 \quad (3.51)$$

with

$$P = \frac{\omega_+^{(2)}}{2} \quad (\text{See Equation (3.37)}) , \quad (3.52)$$

$$Q = \frac{\vec{V}_+^* \vec{Q}}{2\omega_+} = \frac{(V_1^{+*} Q_1 + V_2^{+*} Q_2)}{2\omega_+} \quad (\text{See Equation (3.33)}) , \quad (3.53)$$

and where  $\vec{Q}/2\omega_+ = (Q_1, Q_2)$  is given directly by Equation (3.30) and is reported in Appendix C.



### 3.3.2 Envelope soliton approximate solutions

If  $PQ > 0$  equation (3.51) has an envelope soliton solution

$$A(s_1, t_2) = \mathcal{A} \operatorname{sech}\left[\frac{1}{L_e}(s_1 - u_e t_2)\right] \exp\left[i\frac{u_e}{2P}(s_1 - u_e t_2)\right] \quad (3.54)$$

where

$$\mathcal{A} = \sqrt{\frac{u_e^2 - 2u_e u_c}{2PQ}} \quad (3.55)$$

$$L_e = \frac{2P}{\sqrt{u_e^2 - 2u_e u_c}} \quad (3.56)$$

are respectively the amplitude and the width of the solution.

Once the NLS equation is solved for  $A$  we have  $\sigma_2$ ,  $\vec{\gamma}$ ,  $\vec{\mu}$  and then the complete solution

$$\begin{aligned} y &= \epsilon \left( V_1^+ - i\epsilon V_1^{(1)} \frac{\partial}{\partial x_1} \right) A e^{i\theta} + c.c. \\ &\quad + \epsilon^2 \gamma_{1c} A^2 e^{2i\theta} + c.c. + \epsilon^2 \mu_{1c} |A|^2 + O(\epsilon^3) \end{aligned} \quad (3.57)$$

$$\begin{aligned} \phi &= \epsilon \sigma_{2c} \int |A|^2 dx_1 + \epsilon \left( V_2^+ - i\epsilon V_2^{(1)} \frac{\partial}{\partial x_1} \right) A e^{i\theta} + c.c. \\ &\quad + \epsilon^2 \mu_{2c} \int |A|^2 dx_1 + \epsilon^2 \gamma_{2c} A^2 e^{2i\theta} + c.c. + O(\epsilon^3). \end{aligned} \quad (3.58)$$

where we denote by  $\theta$  the fast phase ( $q_0 n_0 - \omega_+ t_0$ ) and we have omitted the index  $n$  because of the multi scale dependence.

We would like to stress the physical meaning of the d.c.  $O(\epsilon)$  term in angles,  $\sigma_{2c} \int |A|^2 dx_1$ . This term represents one of the major contributions to the solution, and dominates when the reference eigen-vector has a small second component. The fact that it depends on the whole stretching, integrated over the open region, is due to the geometrical constraint: from Figure 2.7 we know in fact that each opening base pair cause an untwist. It is thus normal to find such an integration over all the stretched base pairs: this is a cross check of the validity of the calculation.

The final result can be rewritten introducing explicitly all terms and using continuous coordinates  $x, t$  connected with the multi scale ones by the relations

$x_0 = x, x_1 = \epsilon x, t_0 = t, t_2 = \epsilon^2 t$ . By introducing the quantities

$$\eta = \frac{\epsilon}{L_e} \quad (3.59)$$

$$V_e = \omega_+^{(1)} + \epsilon u_e \quad (3.60)$$

$$V_c = \omega_+^{(1)} + \epsilon u_c \quad (3.61)$$

$$\mathcal{K} = q_0 + \frac{\epsilon u_e}{2P} \quad (3.62)$$

$$\Omega = \omega_+ + \frac{\epsilon u_e}{2P} V_c \quad (3.63)$$

the solution (3.57), (3.58) is then finally written in the following form:

$$\begin{aligned} y &= 2\epsilon V_1^+ \mathcal{A} \operatorname{sech}[\eta(x - V_e t)] \cos(\mathcal{K}x - \Omega t) \\ &+ \epsilon^2 V_1^{(1)} \mathcal{A} \operatorname{sech}[\eta(x - V_e t)] \left[ \frac{-2}{L_e} \tanh(\eta(x - V_e t)) \sin(\mathcal{K}x - \Omega t) + \frac{u_e}{P} \cos(\mathcal{K}x - \Omega t) \right] \\ &+ 2\epsilon^2 \gamma_{1c} \mathcal{A}^2 \operatorname{sech}^2[\eta(x - V_e t)] \cos(2\mathcal{K}x - 2\Omega t) \\ &+ \mu_{1c} \epsilon^2 \mathcal{A}^2 \operatorname{sech}^2[\eta(x - V_e t)] + O(\epsilon^3) \end{aligned} \quad (3.64)$$

$$\begin{aligned} \phi &= \epsilon(\sigma_{2c} + \epsilon\mu_{2c}) L_e \mathcal{A}^2 \tanh(\eta(x - V_e t)) - 2\epsilon \mathcal{A} |V_2^+| \operatorname{sech}[\eta(x - V_e t)] \sin(\mathcal{K}x - \Omega t) \\ &- \epsilon^2 V_2^{(1)} \mathcal{A} \operatorname{sech}[\eta(x - V_e t)] \left[ \frac{2}{L_e} \tanh(\eta(x - V_e t)) \cos(\mathcal{K}x - \Omega t) + \frac{u_e}{P} \sin(\mathcal{K}x - \Omega t) \right] \\ &- 2\epsilon^2 |\gamma_{2c}| \mathcal{A}^2 \operatorname{sech}^2[\eta(x - V_e t)] [\sin(2\mathcal{K}x - 2\Omega t)] + O(\epsilon^3) \end{aligned} \quad (3.65)$$

### 3.4 Existence of solutions and parameter choice: PQ diagrams

We have found the analytical form of the approximate breather like solutions for the *twist-opening* model, which exist if  $PQ$  is positive. We have then to control for what choice of  $q$  and of the frequency branch this is true, to determine which solutions exist, in particular, for our choice of the parameters. Because of the uncertainty in determining the parameter  $G_0$  of the model, we will consider  $G_0$  as a variable, and we will study the sign of  $PQ$  as a function of  $G_0$  and  $q$  on the two branches  $\omega_+(q)$  and  $\omega_-(q)$ .

Equations (3.52) and (3.53) give the values of  $P$  and  $Q$ , together with (3.37) and (C.13), (C.14). Fig. 3.1 shows in bright the regions of the space of parameters  $q$  and  $G_0/(R_0^2 K)$  where  $PQ > 0$ , having fixed the other parameters to their estimated DNA values.

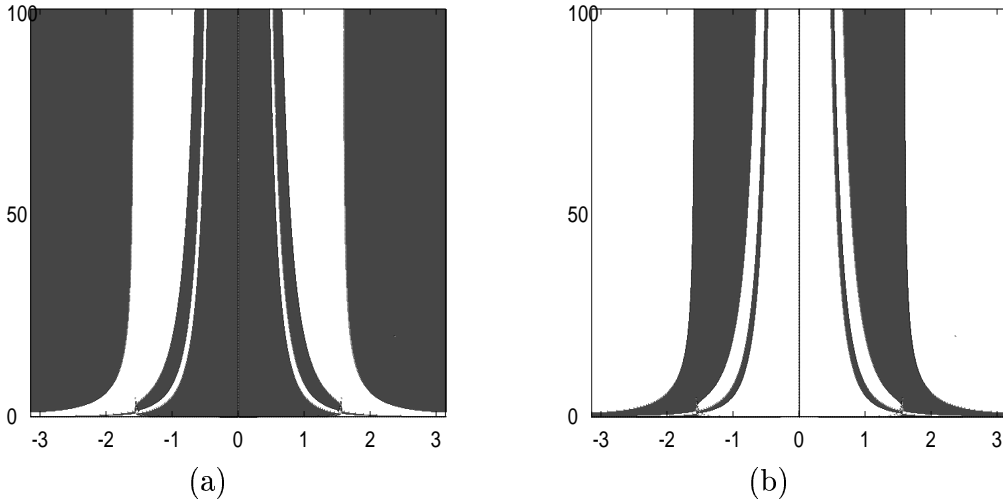


Figure 3.1:  $PQ$  sign as function of the wave number  $q$  (horizontal axis) and of  $G_0/(R_0^2 K)$  (vertical axis). The other parameters are  $D = 0.04 \text{ eV}$ ,  $\alpha = 4.45 \text{ \AA}^{-1}$ ,  $K = 0.04 \text{ eV \AA}^{-2}$ . **(a)**: optical branch, **(b)**: acoustic branch. The bright regions correspond to  $PQ > 0$ , where solution (3.64), (3.65) exists.

### 3.4.1 Small $q$ breathers solutions of the model

#### Bubble-like distortions and small $q$ solutions

Let us come back to the biological meaning of the solutions we are looking for. We remind that the biological phenomenology of reference for what concern the study of breather like solutions is DNA thermal “breathing”, characterized, at room temperatures, by localized oscillating bubbles. Following the interpretation of Peyrard and co-workers, the small “breathing” distortions could act as precursors of the denaturation bubble, accumulating in the promoter regions.

Our aim is to see if our model can reproduce these small bubble-like distortions, *i.e.* distortions characterized by a radial opening that oscillate in time but that is quite regular in space. Furthermore, we are interested in understanding how the coupled radial degree of freedom behaves in correspondence to the radial motion. This means that solutions with high  $q$ , characterized by a fast internal oscillation, have less biological significance in the context of the DNA opening processes of interest.

We focus, then, on the small  $q$  region. From the  $PQ$  diagrams, it results that, for all  $G_0$ , approximate breathers corresponding to the modulation of a wave-packet with small  $q$  arise only if starting from a central modes on the acoustic branch. On the optical branch, solutions exist only for  $q$  greater then a threshold value.  $PQ$  is still positive up to  $|q| = \pi$  if  $G_0 < R_0^2 K$ , or just in an intermediate range for  $G_0$  greater than this value. Other solutions for  $q \rightarrow \pi$  exist on the

acoustic branch if  $G_0 > R_0^2 K$ .

The only small  $q$  solutions are those arising as envelope modulation of a central mode with  $q \approx 0$  on the acoustic branch (i.e.  $\omega = \omega_-$ ). We will consider a different case for what concern the parameter set and we will also change the model Lagrangian, leading to different  $PQ$  diagrams. For the moment, anyway, we will discuss these existing “acoustic” solutions.

### Acoustic mode breathers: analytical solution

Figure 3.3 shows an analytical solution (3.64),(3.65) in the original (not renormalized) displacement and time variables, as a function of  $n$  and  $t$ . The model parameters are fixed at  $D = 0.04 \text{ eV}$ ,  $\alpha = 4.45 \text{ \AA}^{-1}$ ,  $K = 0.04 \text{ eV \AA}^{-2}$ . We use here  $G_0 = 0.5 K R_0^2$ .

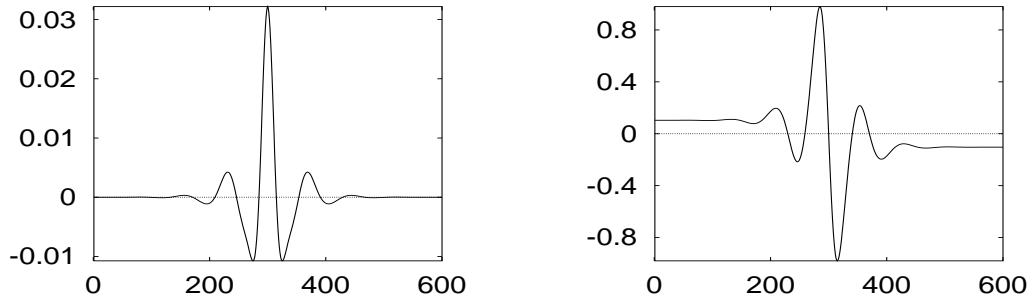


Figure 3.2: Spatial dependence of the radial (left) and angular (right) distortions. (In this picture the chain length is 600  $bps$  and the central site is  $n = 300$ .)

The shape of the radial and angular distortions is reported Figure 3.2. The maximal amplitude of the radial distortion is  $0.032 \text{ \AA}$ . The first two lateral oscillations cover a chain length of 182  $bps$  (distance between the third two zeros starting from the center of the oscillation). The corresponding angular motion contains a kink structure due to the non oscillating term  $\sigma(x, t)$ , that corresponds to the two nonzero asymptotic values of the angle distortion 0.103 and  $-0.103$ . An oscillating part due to the other terms in (3.65) is superimposed on it, so that the angular distortion has a maximal oscillation up to about 0.98 at site 185, and a symmetrical minimum.

Figure 3.3 show for a time interval of 12000  $t.u.$  the radial displacement  $r_n(t) - R_0$  (a) and of the angular displacement  $\varphi_n(t)$  (b), while (c) represents the twist angle, i.e. the difference between neighboring angles,  $\varphi_n(t) - \varphi_{n-1}(t)$ .

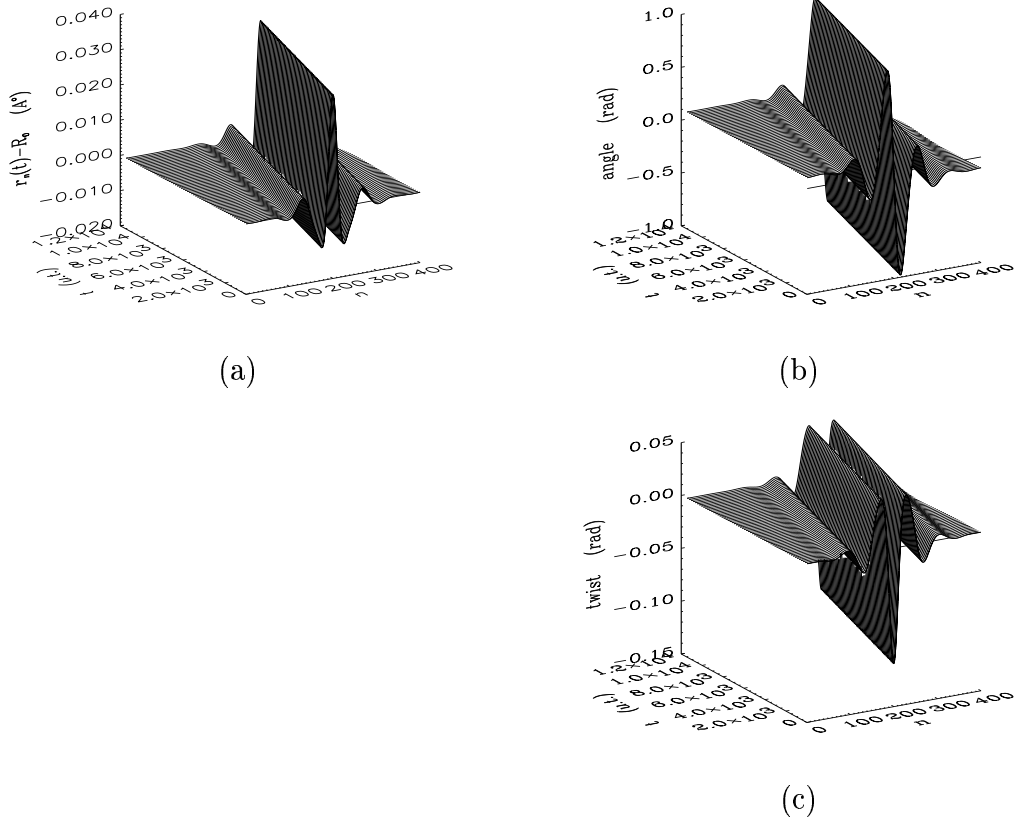


Figure 3.3: Analytical solution (3.64), (3.65). We show here **(a)**: the radial displacement  $r_n(t) - R_0$ , obtained with the parameters indicated below and with  $\epsilon = 0.008$ ,  $u_e = -0.08$ ,  $u_c = 0.1$ ,  $q = 0.1$ . The chain length is of 400 sites. **(b)**: the corresponding angular displacement  $\varphi_n(t)$ . **(c)**: the twist angle, given by the difference between neighboring angles,  $\Delta\varphi_n(t)$ . The total time is  $12000 t.u.$

The shape of the solution agrees with the geometrical properties of the molecule related to its helicoidal structure and shows, as expected, that our model can indeed describe the local untwisting which should be coupled with the radial opening due to the geometrical constraints.

We plot in Figure 3.3 (c) the evolution of the twist angle. In addition to the local untwist, overtwists on the boundaries are visible. They derive from the oscillating part of the solutions.

The local twist distortion is of the order of  $-0.15$ . We stress that the corresponding twisting number  $\sigma = \Delta\Theta/\Theta_0$  results to be of the order of 0.25, and thus we are out of the range where the fixed planes approximation discussed in Section 2.5 can be considered to be valid on the basis of the experimental results on twist-stretch couplings for single DNA molecules [6]<sup>2</sup>.

<sup>2</sup>This do not necessarily implies that the fixed planes approximation *is* actually not valid,

V

The coupled breather and kink solutions move with a peak velocity  $V_e = V + \epsilon u_e \approx 9.60 \cdot 10^{-3} \text{ bps}/t.u.$ . The group velocity is  $V = \omega^{(1)} \approx 9.60 \text{ bps}/t.u.$ . It actually has an internal degree of freedom, in the sense that its shape change with time, due to the oscillating terms in  $(\mathcal{K}x - \Omega t)$  and in  $2(\mathcal{K}x - \Omega t)$ , see Equations (3.64), (3.65). The characteristic frequency of the oscillation is small:  $\Omega = \omega_- + (\epsilon u_e/2P)V_c \approx 7.6 \cdot 10^{-4} t.u.^{-1}$ , (while  $\omega_- \approx 9.6 \cdot 10^{-4} t.u.^{-1}$ ). The correspondent oscillation period is about  $8230 t.u.$ . Anyway, in this case, the phase velocity of the internal oscillation,  $\Omega/\mathcal{K} = 9.55 \cdot 10^{-3} \text{ bps}/t.u.$ , is very close to the peak velocity  $V_e \approx 9.60 \cdot 10^{-3} \text{ bps}/t.u.$  of the envelope, so that the envelope and the sinusoid maxima move together. The period of the solution is, actually, about  $1.6 \cdot 10^6 t.u.$

### Acoustic mode breather: numerical integration

We now consider the analytical solution given by Equations (3.64), (3.65), and shown in Figure 3.3, as approximate solution of the complete equations of motion. If we deal with small enough amplitudes, the analytical solution can be used as an initial condition for a direct integration of the true equations of motion of the model. Even if the analytical solution is obtained on the basis of the approximated equations of motion (2.39), (2.40), we use here the complete equations of motion, derived from the full Lagrangian (2.20). We perform then a numerical integration of the equations of motion, using a fourth order Runge-Kutta algorithm.

The long time evolution of the initial condition, calculated with the full Lagrangian and shown in Figure 3.4, attests that the local excitation is quite stable: during all the simulation time the total energy loss due to the absorbing conditions is about 0.5% of the total energy. The functional shape is well maintained with the exception of a local distortion of the radial part which arises near the initial peak position.

We finally stress that, for the breathers arising from acoustic modes we have described, the breather frequency  $\Omega$  *does not* lie in the linear frequency gap but is in the acoustic band. Therefore, the breathers so obtained should not be stable in principle. A numerical stability analysis would confirm this fact with certainty. Anyway, a longer simulation show that the energy loss at the boundaries will increase at later times: it is of about the 3% at  $t = 18000 t.u.$ . These approximate solutions can travel for a certain distance without losing their shape, but will be probably destroyed after a certain time.

---

because in those experiments DNA does not preserve its straight conformation for large  $\sigma$  values, so that a direct comparison is impossible. Anyway, in the case of large twist distortions, we have not reference data to confirm that the fixed planes approximation is valid.

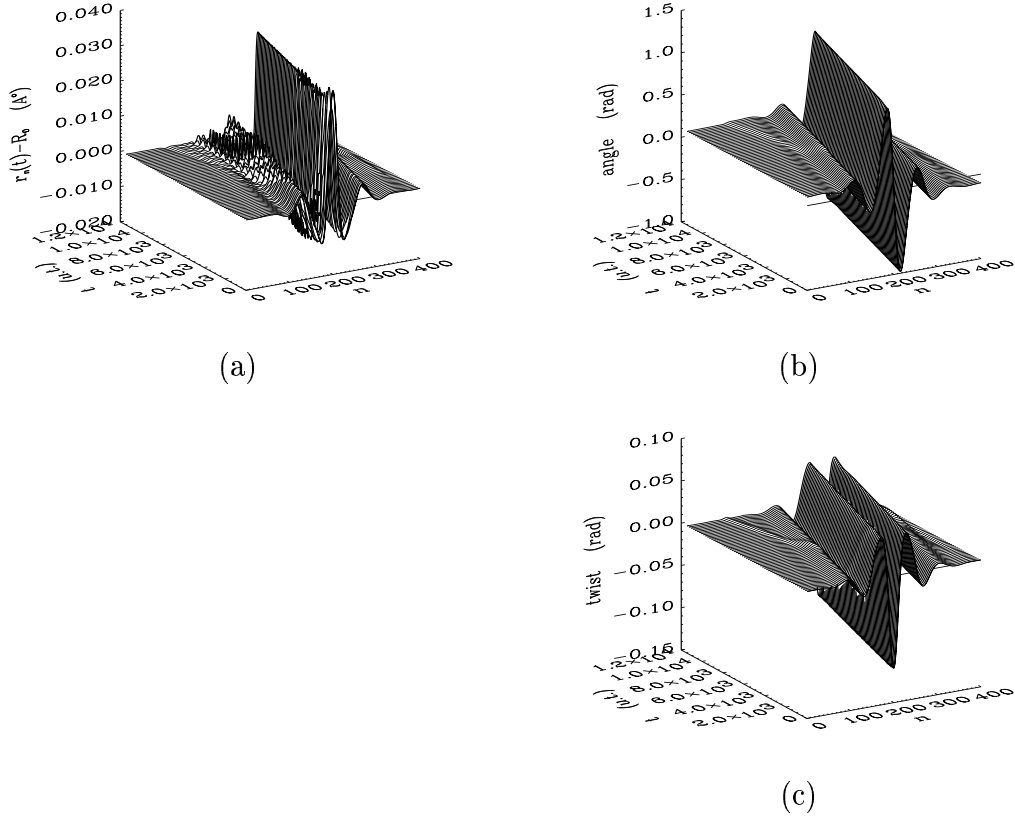


Figure 3.4: Results of numerical integration of the equations of motion with the same parameters and initial conditions of the previous figure. (a): the radial displacement  $r_n(t) - R_0$ ; (b): the corresponding angular displacement  $\varphi_n(t)$ . (c): the twist angle. The total integration time is  $12000 t.u.$ , the chain length is  $400 bps$ . We use absorbing boundary conditions.

## 3.5 A “breathing” solution obtained with a different set of parameters

### 3.5.1 A small amplitude solution

#### Analytical solution

It is interesting to see what kind of solution one can obtain by changing parameters in an adequate way. In particular it is interesting to know if a breathing bubble-like solution of the desired type can exist in some region of the parameter space. We will show one similar solution, discussing its main features and stability.

Increasing the value of  $K$  to  $1 eV \text{Å}^{-2}$ , without changing  $D$  and  $\alpha$ , we obtain

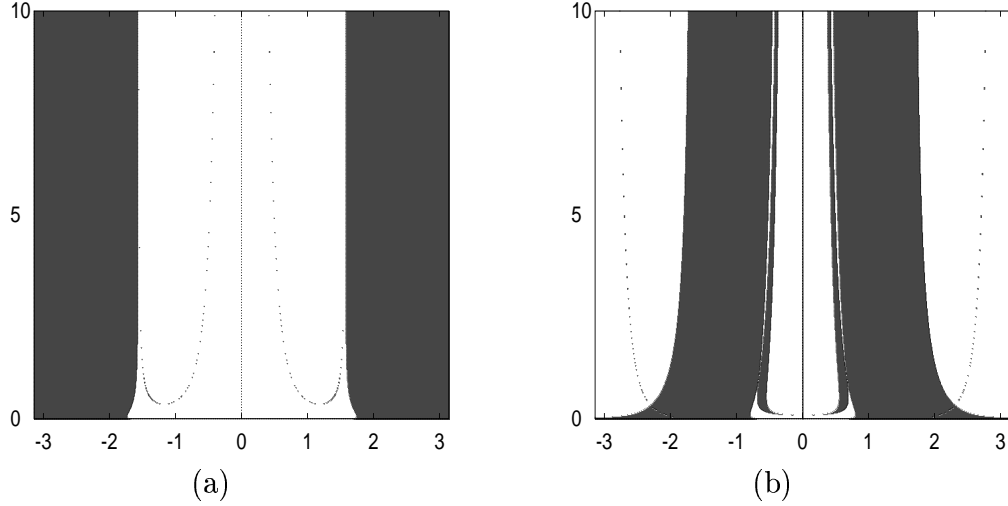


Figure 3.5:  $PQ$  sign as function of the wave number  $q$  (horizontal axis) and of  $G_0/(R_0^2 K)$  (vertical axis) for  $K = 1 \text{ eV \AA}^{-2}$ . The other parameters are  $D = 0.04 \text{ eV}$ ,  $\alpha = 4.45 \text{ \AA}^{-1}$ . **(a)**: optical branch, **(b)**: acoustic branch.

the diagrams showing the  $PQ$  sign as a function of  $q$  and  $G_0$  shown in Figure 3.5. In this case, the breather approximate solutions obtained starting with a mode on the optical branch exist, in the small  $q$  range.

We take  $G_0 = 0.5 R_0^2 K$  and we consider a solution with  $q = 0.1$ ,  $\omega = \omega_+(q) = 0.061 \text{ t.u.}^{-1}$ , and with  $\epsilon$ ,  $u_e$ ,  $u_c$  as indicated in Figure 3.7. The spatial shape of the solution is reported in Figure 3.6, the time evolution in Figure 3.7.

As in the previous case, we first show, in Figure 3.7, the behavior of the analytical solution, during a short time lapse. The solution is shown in the original unrenormalized variables in a chain of 300 bps. The total time interval corresponds to a few internal oscillations. The spatially localized, oscillating radial solution, and the coupled, non oscillating angular part can be recognized. There are, in addition, smaller oscillations corresponding to corrections of the next perturbation order.

For what concerns the radial displacement, the typical breather oscillation is clearly visible; its period  $2\pi/\Omega$  is of  $104.7 \text{ t.u.}$ . The amplitude  $2\epsilon\mathcal{A}/\alpha$  and the half height width, which is about  $2.77L_e/\epsilon$ , are respectively  $0.016 \text{ \AA}$  and  $20 \text{ bps}$ .

The main contribution to the corresponding angular displacement  $\varphi_n(t)$  is the kink-like term  $\epsilon\sigma_c L_e \mathcal{A}^2 \tanh(\eta(x - V_e t))$  of (3.65). We stress again that the kink-like deformation in the angles corresponds to an untwist, which moves together with the breather along the chain. This can be seen in the third graph of Figure 3.7, where the differences  $\varphi_n - \varphi_{n-1}$  have been plotted. The resulting untwist is of about  $4 \cdot 10^{-4}$ , and corresponds to  $\sigma \approx 10^{-3}$ . In this case the fixed plane approximation is likely to be valid.



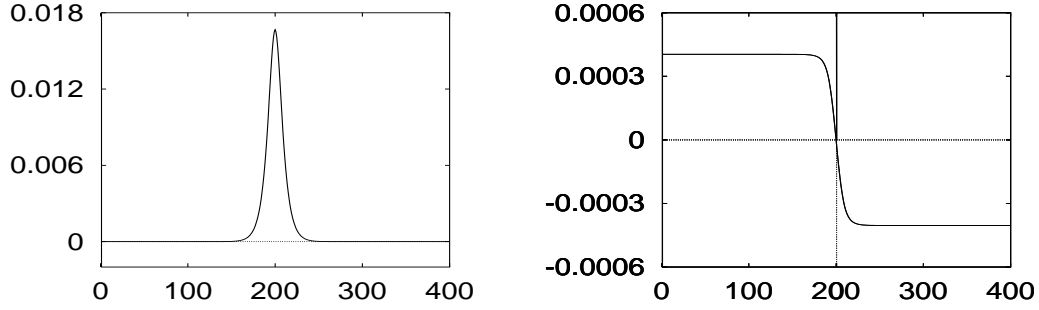


Figure 3.6: Spatial dependence of the radial (left) and angular (right) distortions. (Here the chain length  $400 \text{ bps}$ , the central site  $n = 200$ .)

### Numerical integration results

We report in Figure 3.8 the result of the integration of the equation of motion with initial conditions which correspond to the analytical solution of Figure 3.7. The amplitude and width parameters preserve their initial values with good accuracy. We numerically found for  $2\epsilon\mathcal{A}$  the value  $0.017 \pm 0.001 \text{ \AA}$ . We also numerically evaluate the oscillation period, that results to be  $106.2 \pm 0.1 \text{ t.u.}$  The slight discrepancy between the theoretical and measured values depends on the approximation, *i.e.* on the fact that the analytical solution (3.64), (3.65) is only an approximate solution of the equations of motion.

The total simulation time corresponds to more than  $2.2 \cdot 10^3$  oscillation periods. We introduce here absorbing boundary conditions to avoid noise effects produced by reflection of the small amount of radiated energy. The evaluation of the total absorption of energy at the chain boundaries shows that the derived analytical functions are in fact quasi-solutions of the model: they maintain their stability for long times with a total energy loss that is less than  $10^{-5}$  of the total initial excitation energy.

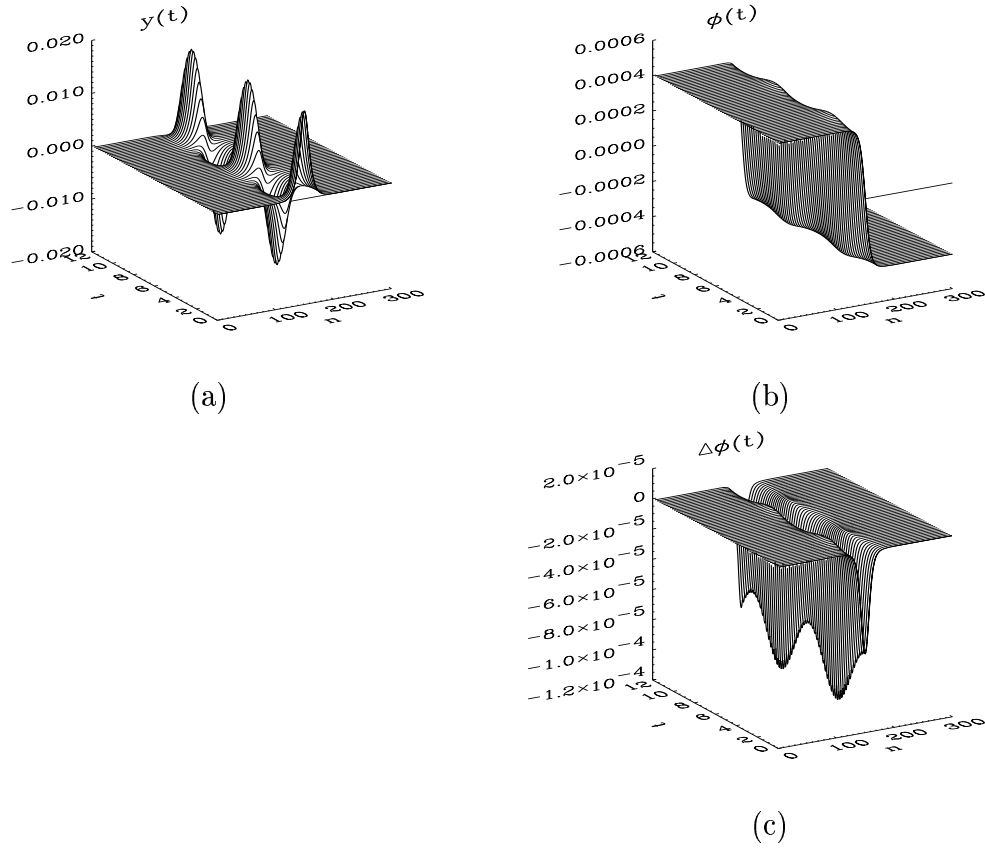
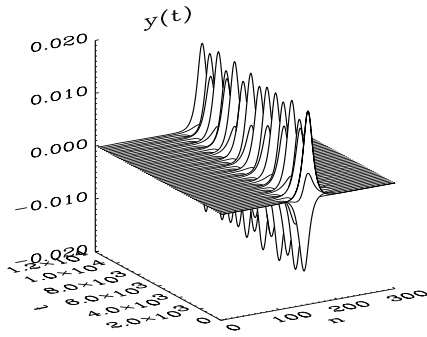
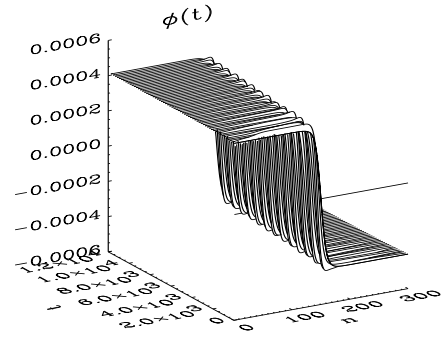


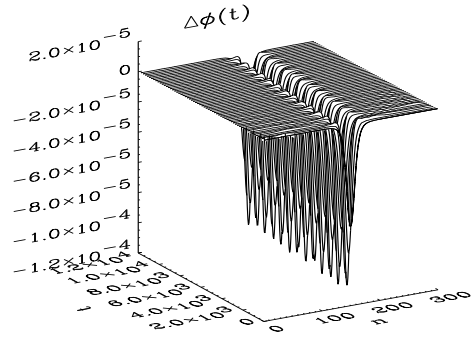
Figure 3.7: Analytical solution (3.64), (3.65) in the case  $K = 1$ . We show here **(a)**: the radial displacement  $r_n(t) - R_0$ , obtained with the introduced model parameters and with  $\epsilon = 0.1$ ,  $u_e = -0.1$ ,  $u_c = 0.1$ . **(b)**: the corresponding angular displacement  $\varphi_n(t)$ . **(c)**: the twist angle. The chain length is 300 *bps*, the total time 250 *t.u.*



(a)



(b)



(c)

Figure 3.8: Numerical integration of the initial condition which corresponds to the analytical solution of Figure 3.7. **(a)**: radial displacement  $r_n(t) - R_0$ ; **(b)**: angular displacement  $\varphi_n(t)$  generated by the numerical integration of the same initial conditions; **(c)**: twist angle.

### 3.5.2 Solution with larger amplitude and limit of validity of the approximation

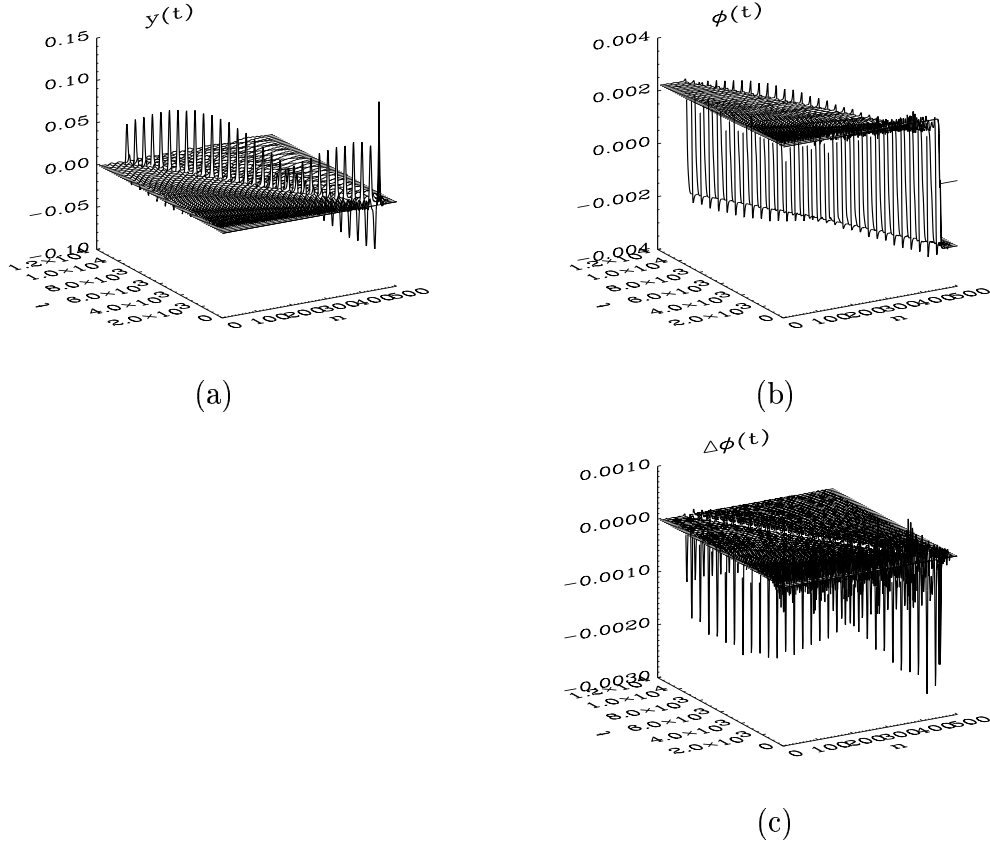


Figure 3.9: Numerical integration of an initial condition obtain with solution parameters  $\epsilon = 0.2$ ,  $u_e = -0.2$ ,  $u_c = 0.6$ . We perform again the simulation with absorbing boundary conditions. **(a)**: radial displacement  $r_n(t) - R_0$ ; **(b)**: angular displacement  $\varphi_n(t)$  generated by the numerical integration of the same initial conditions; **(c)**: twist angle. (We stress that the apparent slow modulation of the maximum amplitudes is also due to the beating between the actual oscillation and the sampling time, as the apparent oscillation period.)

As our solution has been obtained with a Multiple Scale Expansion, we should not expect it to be a good solution when its amplitude increases to much. This can be seen on the results of a numerical simulation starting from a much larger amplitude (Figure 3.9). The initial radial amplitude is  $2\epsilon\mathcal{A} = 0.098 \text{ \AA}$  and the half height width  $2.77L_e/\epsilon \sim 4 \text{ bps}$ . This initial solution is not stable: it decays very fast and radiates energy before stabilizing to a breather which has still a pretty high amplitude ( $\sim 0.072 \pm 0.005 \text{ \AA}$ ) and which is localized on about 6 sites (half height width). Although it is very narrow, the breather is still

mobile in the system and it is accompanied by a sharp kink as expected from the geometrical constraints. The solution reached after the transient is stable as shown in Figure 3.10, where we plot the total system energy as a function of time. The energy tends to stabilize, after the period during which the waves emitted because of the initial solution decay are absorbed by the ends.

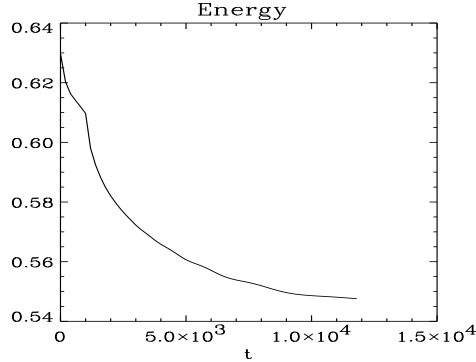


Figure 3.10: Total system energy during the simulation with parameters as in Figure 3.9.

Approximate solutions with a sufficiently small amplitude are in the linear approximation regime. In this regime, the envelope function becomes flatter and extends over a larger chain length, so that the wave-packet becomes essentially indistinguishable from a linear phonon mode, described by a single wave number  $q$  and its relative linear frequency  $\omega_{\pm}$ . Among the effects of nonlinearity, which arise for distortions with a slightly greater amplitude, is the change of the oscillation frequency: for a fixed  $q$ , the new  $\Omega = \omega_{\pm} + (\epsilon u_e/2P)V_c$  will differ from the linear value.

In the case of breathers arising from the small  $q$  region of the optical branch discussed in this section, we always have  $\Omega < \omega_+$ , so that  $\Omega$  always lies in the frequency gap between the two branches. As we already discussed, this is a necessary condition for the existence of breathers, which prevents from resonant energy exchange with phonons.

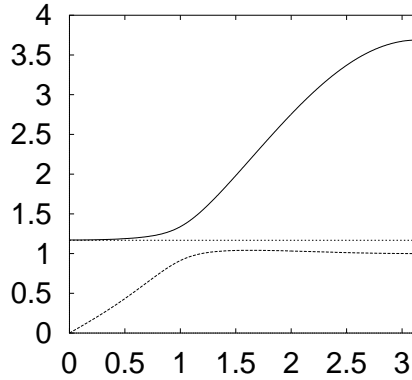


Figure 3.11: Linear frequencies  $\omega_+$  and  $\omega_-$  and breather frequency  $\Omega$  for a choice of model and solution parameters as in Figure 3.7. (The picture refers to the rescaled system).

### 3.6 First conclusions: acoustic solutions do not reproduce the “breathing” of DNA

With the present model and parameter choice we have only the kind of solutions displayed in Figures 3.3 and 3.4. It is not a good solution from a biological point of view. First of all, we have pointed out that, being the local twist distortion of the order of  $-0.15$ , the twisting number  $\sigma = \Delta\Theta/\Theta_0$  results to be out of the range where the fixed planes approximation discussed in Section 2.5 can be considered to be valid on the basis of the experimental results [6].

Moreover, the spatial extension of the solution is quite large with respect to breathing modes excitations and also with respect to transcription bubbles (which have dimensions of the order of  $20\text{ bps}$ ). Furthermore, even if  $q$  is small, the solution shows several oscillations along the chain, and it is thus quite different from the simple bubble-like distortion we were looking for. The shape of the solution depends of course on the parameters. Anyway, from (3.55) we know that amplitude and width of the envelope function, and thus of the solution, are inversely proportional. A narrower radial distortion will be able to select just a central oscillation, and then will be more similar to a bubble deformation, but at the same time it will correspond to a larger distortion. Unfortunately, being our solutions (3.64), (3.65) just approximate solution obtained with a Multiple Scale Expansion, they will become unstable if their amplitude is too large. Actually, the solution shown in the previous figures already corresponds to the boundaries of the allowed solutions. Larger analytical solutions obtained with the expansion technique suddenly loose their shape - usually being pinned in the initial position due to discreteness effects.

The inadequate shape is not the only defect of the solutions we have found.

We remind that the experimental estimation of the oscillation frequency of small amplitude breathing motions in real DNA is of the order of  $10^{-12} \div 10^{-13}$  *sec*.

Having considered a mode on the acoustic branch, our solution oscillate very slowly. The frequency of solutions (3.64), (3.65) is in fact, in this case,  $\Omega = \omega_- + (\epsilon u_e/2P)V_c$ , as given by (3.59), with  $\omega_- \rightarrow 0$  if  $q \rightarrow 0$ .

Of course, this depends on the choice of the parameters, that determines the  $PQ > 0$  regions and then the range of existence of the various solutions. We stress anyway that  $G_0$  is the only parameter for which even a choice of the order of magnitude represents a true problem, but this does not change the  $PQ$  sign near  $q \approx 0$ , as displayed in Figure 3.1.

*We have then to conclude that the twist-opening model, with the parameters we choose, does not sustain appropriate oscillating solutions which could mimic the experimentally observed “breathing” modes in DNA.* This consideration could lead, at first sight, to different conclusions:

1. the parameter set we choose for the model is not correct;
2. the model does not really mimic DNA in a good way, so:
  - (a) the structure of the model is not correct, and we have to improve it;
  - (b) there are some missing interactions that have to be included in our description;
  - (c) the hypotheses made by Peyrard and Bishop on the specific dynamical features leading to bubble formation are incorrect and the introduction of a more realistic geometry could demonstrate this fact.

We will now discuss the previous conclusions.

*Errors in the determination of the constants.*

For what concerns the first hypothesis, we cannot completely exclude errors in the way we choose the model parameters, and we recall that we are not able to fix a value for  $G_0$ . As shown in Section 3.5, with a different choice of the constant  $K$ , for instance, we can recover “optical” breathers of the interesting type. Anyway, we have shown in Section 2.5 that at least the order of magnitude of the various parameters can be fixed with good accuracy, on the basis of experimental results on real DNA. Furthermore we already claimed in several parts of this Thesis that  $G_0$  has only a minor effect in determining the solution arising from the expansion in multiple scales. In particular, we want to stress that the  $PQ$  value in correspondence of the optical branch for small  $q$  is negative for a very large range of  $G_0$  (up to  $G_0 = 100R_0^2K$  and bigger). It is thus quite unlikely that a more accurate determination of the set of parameters could dramatically change the results presented in this section.

*Errors in modeling DNA.*

The hypothesis of a model inaccuracy in reproducing DNA dynamics is quite probable. To conclude, on the basis of these results, that the PB description of the breathing modes of DNA and of the bubble formation is wrong, is obviously not correct. The PB model and the *twist-opening* model are strongly simplified and it is possible that the first one, even if it is simpler, contains some specific physical features that are lost for some reason in the second one. We think that if there is an error in our model, it should be in the kind of interaction we included, and not in the model structure, that we reconstruct by referring to the basic DNA geometry.

In particular, the coupling between neighboring bases along the strand has a very different form in the two models. This coupling represents the quite complex set of interactions which compose the stacking force, that is actually difficult to be reproduce. The PB model includes as stacking term an interaction attributed to the overlap of  $\pi$  electrons on base pairs. This interaction is different from the interaction due to the strands: we think then that an accurate rediscussion of the stacking interaction terms is necessary. *In the next section, we will propose a very simple improvement of the twist-opening model, justified on the basis of some known properties of stacking, which leads to recover the existence of oscillating breather solutions of the desired type.*

## 3.7 How to improve the model to recover oscillating breather solutions

The defects of the *twist-opening* model can be removed by a simple improvement, obtained by adding one term to Lagrangian (2.20). We will describe in this section which physical features of real DNA chains have to be included in the model and how it can be done in a simple way.

Then we study the effect of the new term: first of all, we apply the expansion technique developed in the first part of this chapter to the improved model. This can be done with a minimum effort, due to the operatorial formalism we have introduced. We will find that the new model admits oscillating breathers that can better represent the “breathing” of DNA. We will then test the stability of these approximate solutions by using them as initial condition for the complete equations of motion, as we already did above.

### 3.7.1 A new stacking term

#### Addition of $W_{stack}$ to the Lagrangian

To understand how the *twist-opening* model can be conveniently improved in order to obtain more realistic breathers, we will go back to its Lagrangian (2.20).



We can then ask whether its structure is actually able to reproduce the main physical features of the DNA duplex.

We focus on the stacking interaction. In DNA, stacking arises, as we have discussed in Chapter 2, from many different interactions. Its overall action is to favor the relative position of neighboring base pairs in the equilibrium double helix configuration, as if they were special construction bricks with one way to combine together. Our idea was that the combined effect of fixed base pair planes, elastic rod coupling along the strands and Morse potential coupling between the bases in each pair could be sufficient to mimic the resulting effect of these interactions, by *stacking* the base pairs in their equilibrium positions. Anyway, this was obviously a strong simplification.

Authors of the PB model consider as a main stacking term the effect arising from the overlap between  $\pi$  electrons of the base pairs. The interaction between electronic clouds tends to favor the opening of pairs which are close to an opened one. PB studies [33] show that base pairs situated on the boundaries of an open bubble, in fact, have a greater probability to open with respect to base pairs in a closed region. This is due to the stabilizing effect of stacking interaction with neighboring base pairs, which is removed when a neighboring pair is out of its equilibrium configuration.

Consider now the approximated Lagrangian of the *twist-opening* model, Equation (2.37). For small radial displacements, the interaction between neighboring distortion in that Lagrangian is represented only by terms of the form

$$(y_n + y_{n-1})^2. \quad (3.66)$$

With such an interaction the opening of a base pair induces in the neighbors the tendency to *close*, a mechanism which goes into the opposite direction with respect to the one described above.

It is thus natural to try to improve the model by adding a term which balances this effect by enhancing opening of base pairs on a bubble boundary. We simply introduce in (2.20) one more linear potential term of the type:

$$W_{stack} = \sum_n S(r_n - r_{n-1})^2 = \sum_n S(y_n - y_{n-1})^2. \quad (3.67)$$

The introduction of the new potential adds one more parameter, the constant  $S$ , to be determined. Furthermore, this will imply a rediscussion of the choice of the parameter set, because  $W_{rods}$ ,  $W_{stack}$  and  $W_{cur}$  are all related to the coupling along the helix, and thus by the stacking interaction. We will not discuss here how to determine the values of the constants: we will deal with this problem in our future work.

We write for clarity the extended Lagrangian of the model, obtained by introducing the direct stacking term:

$$\mathcal{L} = E_{kin} - V_m - W_{rods} - W_{cur} - W_{stack} \quad (3.68)$$

$$\begin{aligned} &= \sum_n (m\dot{r}_n^2 + mr_n^2\dot{\varphi}_n^2) - D(e^{-\alpha(r_n - R_0)} - 1)^2 \\ &- \sum_n K(\sqrt{h^2 + r_{n-1}^2 + r_n^2 - 2r_{n-1}r_n \cos(\varphi_n - \varphi_{n-1})} - L)^2 \\ &- \sum_n G_0(\varphi_{n+1} + \varphi_{n-1} - 2\varphi_n)^2 - \sum_n S(y_n - y_{n-1})^2. \end{aligned} \quad (3.69)$$

### 3.7.2 Analytical solution on the optical branch

#### The optical branch curvature at $q = 0$

The existence of approximate breathers with a central mode in the small  $q$  region of the optical branch depends on the sign of  $PQ$ . We know furthermore that their stability is related to the fact that, by increasing the amplitude of a solution out of the linear range, its frequency changes, with respect to the corresponding linear one. If the new frequency ( $\Omega = \omega_+ + (\epsilon u_e/2P)V_c$ ) lies out of the phonon band, the breather cannot spread out by phonon resonance and remains stable. For small  $q$ , this will depend on the curvature of the dispersion curve  $\omega_+(q)$  at  $q = 0$  and on the sign of  $\Omega - \omega_+$ . Dispersion curves curvature and breather stability are in fact correlated, because the curvature of a branch determines, *e.g.*, whether a decrease of  $\Omega$  will make the breather frequency enter in the phonon gap, or in the phonon band.

For the *twist-opening* model, with  $G_0$  values in the interval  $]0 \div 100] R_0^2 K$  and with the usual choice of other parameters, the value of  $Q$  turns out to be positive. The sign of  $PQ$  is thus determined by the sign of  $P$ , which enters also in the determination of the sign of  $\Omega - \omega_+$ .

In our original model, for  $K = .04 \text{ eV \AA}^{-2}$ , the upper branch has negative curvature (see Figure 2.10). The case with  $K = 1 \text{ eV \AA}^{-2}$ , which possesses optical breather solutions, has instead inverted curvature of the upper branch (see Figure 3.11).

Inserting the new stacking term, we calculate that, for all values of  $G_0$ , the optical branch curvature at  $q = 0$  is positive, provided that  $S$  is over a small threshold of about  $0.06K$ . This gives a good indication that the properties of the system for small  $q$  are changed by the introduction of  $W_{stack}$ .

In order to perform some first studies on the improved model we choose  $S = 2K$ . Figure 3.12 shows how the dispersion curves are changed by the introduction of the direct stacking term, for the same four values of  $G_0$  we had previously (see Figures 2.10).

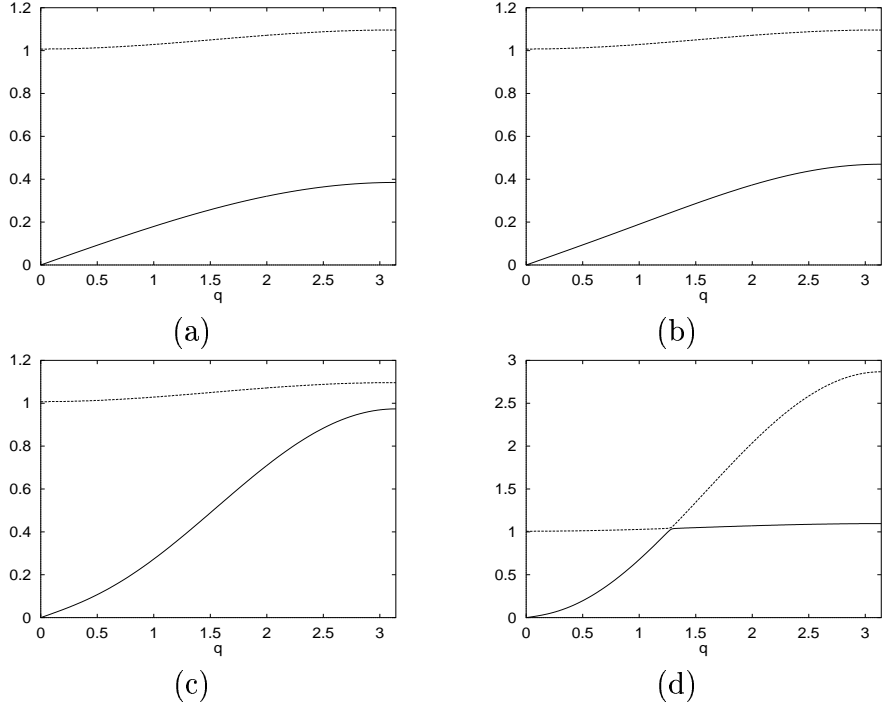


Figure 3.12: Dispersion curves for the model with the added stacking term, with  $S = 2K$ , for various choices of the parameter  $G_0$ : **(a)**:  $G_0 = 0.01KR_0^2$  **(b)**:  $G_0 = 0.1KR_0^2$  **(c)**:  $G_0 = KR_0^2$  **(d)**:  $G_0 = 10KR_0^2$  The other model parameter are fixed at  $D = 0.04 \text{ eV}$ ,  $\alpha = 4.45 \text{ \AA}^{-1}$ ,  $K = .04 \text{ eV \AA}^{-2}$ .

### The $PQ$ diagrams

Let us focus on the case  $S = 2K$ , and look at the  $PQ$  diagrams of the improved model. They are reported in Figure 3.13. In the small wave number region, *we can have breather solutions through the multiple scale expansion technique both in the optical and in the acoustic branch*. The addition of the new term actually leads to the existence of interesting approximate oscillating solutions.

### The analytical solution

The expansion technique developed in Chapter 3 allows a quick calculation of breather solutions with the extended Lagrangian. Due to the general formalism we have used, the new (linear) potential  $W_{stack}$  can be directly introduced in the previous calculations as one more term in the linear part of the equations. More explicitly, the new  $S(y_n - y_{n-1})$  term simply corresponds to an additional part

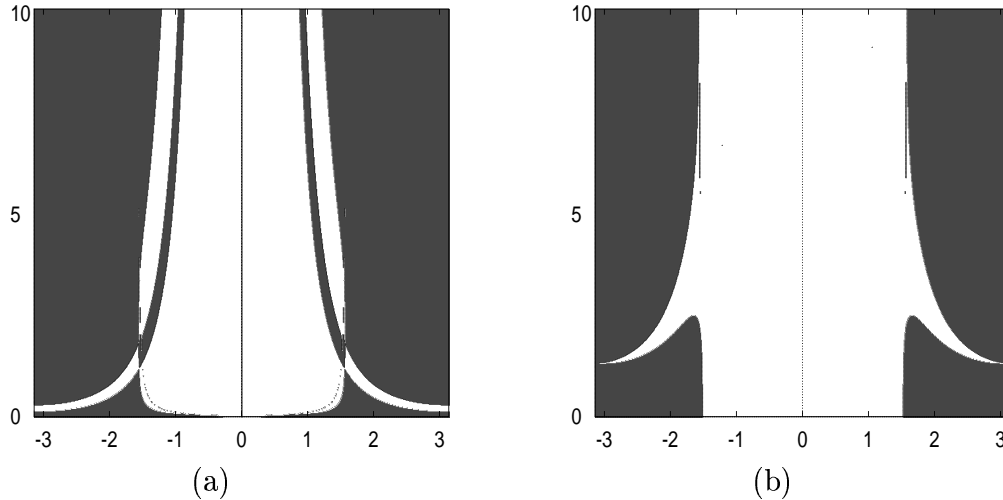


Figure 3.13:  $PQ$  sign as function of the wave number  $q$  (horizontal axis) and of  $G_0/(R_0^2 K)$  (vertical axis) for the model whit stacking  $S = 2K$ . The parameters are  $D = 0.04 \text{ eV}$ ,  $\alpha = 4.45 \text{ \AA}^{-1}$ ,  $K = 0.04 \text{ eV \AA}^{-2}$ . (a): optical branch, (b): acoustic branch. The bright regions correspond to  $PQ > 0$ .

$S(1 - \cos(q))$  in the (1, 1) component of matrix  $\hat{J}(q)$ :

$$\hat{J}(q) = \begin{pmatrix} a(q) & c(q) \\ c^*(q) & b(q) \end{pmatrix} \doteq \begin{pmatrix} 1 + 2K_{yy}(1 + \cos q) & iK_{y\phi} \sin q \\ +S(1 - \cos(q)) & \\ -iK_{y\phi} \sin q & 2K_{\phi\phi}(1 - \cos q) \\ & +G(6 - 8 \cos q + 2 \cos 2q) \end{pmatrix} \quad (3.70)$$

The resulting solution has the general form already given in Equations (3.64) and (3.65): note in fact that the nonlinear part of the calculation is not affected by the introduction of  $W_{stack}$ , and that  $Q$  remains unchanged. Once having added this term to  $\hat{J}(q)$ , *i.e.* once redefined  $a(q)$ , Equations (2.48) and (2.49) for the order  $\epsilon$ , (3.34), (3.35) and (3.36) for the order  $\epsilon^2$  and (3.37) for the order  $\epsilon^3$  can be directly applied to find the new eigenvectors  $\vec{V}^\pm$ , the correction to the interesting one  $\vec{V}^{(1)}$  and the  $P$  parameter in the NLS equation determining the envelope  $A$ . Formally, Equations (3.64) and (3.65), defining the solution  $y_n(t), \phi_n(t)$ , still hold unchanged.

Figure 3.14 shows the analytical solution  $y_n(t), \phi_n(t)$  obtained with the improved model starting from a central mode  $q = 0.1$ ,  $\omega_+(q) = 5.18 \cdot 10^{-2} \text{ t.u.}^{-1}$  and with the parameter values reported in the figure caption. The maximal amplitude of the radial displacement is of about  $0.0255 \text{ \AA}$ , the width at half height of about  $8 \text{ bps}$ . The angular kink ranges between  $\pm 3.8 \cdot 10^{-4}$  and corresponds to a maximal twist distortion of about  $1.3 \cdot 10^{-4}$ . The breather frequency

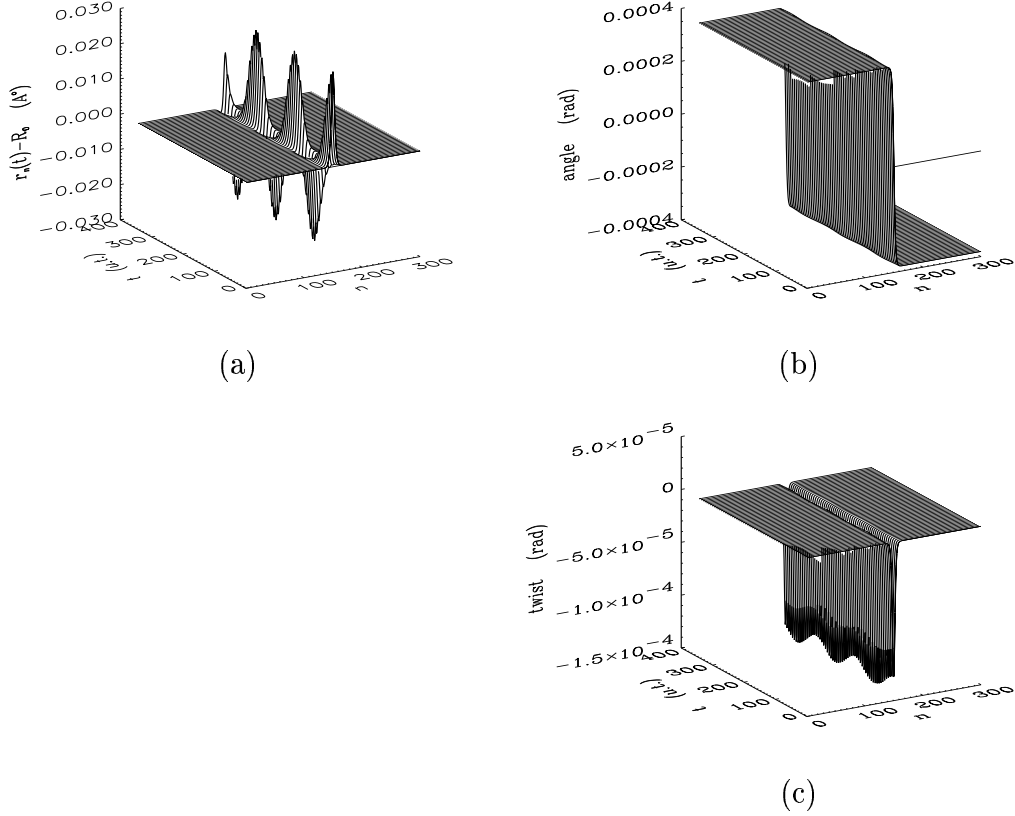


Figure 3.14: Analytical solution (3.64), (3.65) for the improved model with  $S = 2K$ ,  $G_0 = 0.5R_0^2K$ , obtained with parameters  $\epsilon = 0.1$ ,  $u_e = -0.1$ ,  $u_c = 0.1$ . **(a)**: radial displacement  $r_n(t) - R_0$ ; **(b)**: corresponding angular displacement  $\varphi_n(t)$ ; **(c)**: twist angle. The chain length is 300 *bps*, the total time 250 *t.u.*

is  $\Omega = 5.16 \cdot 10^{-2} t.u.^{-1}$ , corresponding to a period of about 121.7 *t.u.* Note that this is of the order of  $10^{-12}$  *sec* and fits the experimental data on the order of magnitude of the characteristic time of DNA “breathing”. The distortion moves with a velocity  $V_e = V + \epsilon u_e \approx 2.73 \cdot 10^{-4}$  *bps/t.u.*

### 3.7.3 Numerical simulation of the new solution

The stability of the approximate solution displayed in Figure 3.14 has to be tested by the numerical integration of the equations of motion obtained with the new Lagrangian (3.68), with initial condition given by the analytical solution itself. We have integrated for a time of about 233500 *t.u.*, corresponding to about 1900 oscillation periods. Results are shown in Figure 3.15. We recall that the apparent oscillation period is due to the beating between the actual oscillation

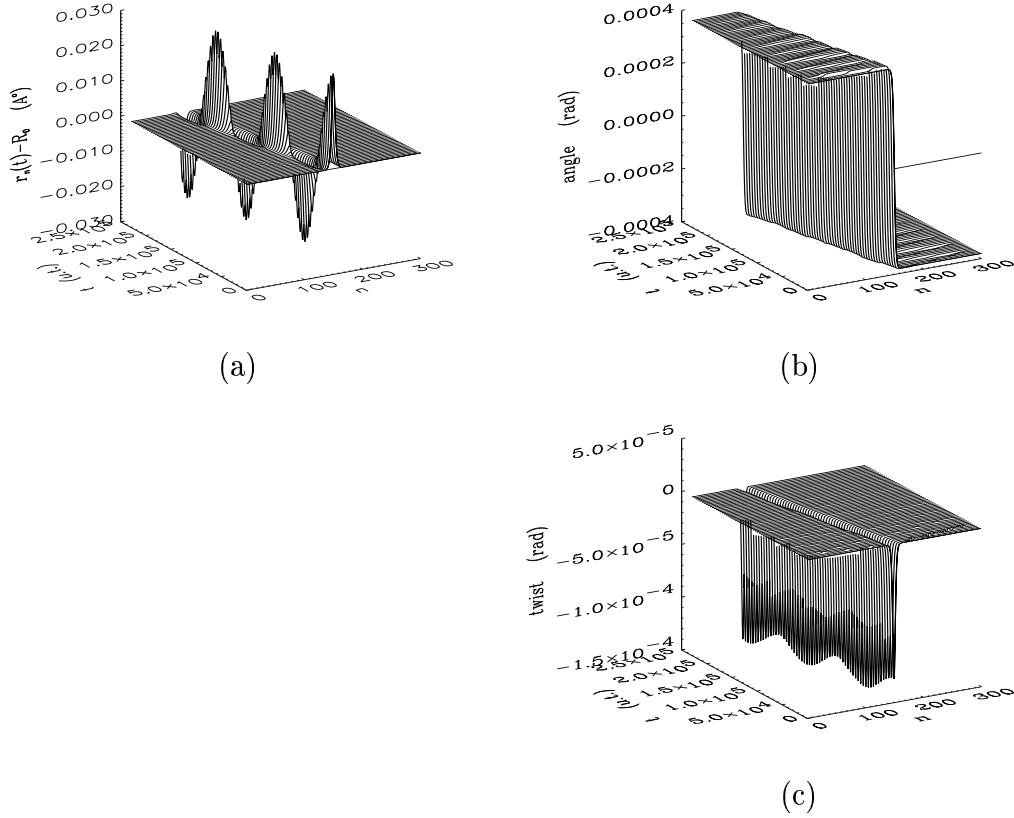


Figure 3.15: Numerical integration of the initial condition which corresponds to the analytical solution of Figure 3.14. **(a)**: radial displacement  $r_n(t) - R_0$ ; **(b)**: angular displacement  $\varphi_n(t)$ ; **(c)**: twist angle.

and the sampling time.

We have measured the period of the oscillations and found  $121.7 \pm 0.1 t.u.$  in agreement with the theoretical value. The radial amplitude is of  $0.026 \pm 0.001 \text{ \AA}$ , and the peak velocity  $2.70 \pm 0.02 \cdot 10^{-4} bps/t.u.$

These numerical results and Figure 3.15 show that the breather+kink solution found by the multiscale expansion is a very good approximate solution for the improved model, and is characterized by a strong stability. Even using absorbing boundary conditions, we do not register any energy variation up to the order  $10^{-10}$  during all the simulation time, showing that the breather does not loose energy.

We also would like to point out that the relative high amplitude, that could be probably increased remaining in the approximation range, and the frequency quite similar to the measured frequencies for DNA “breathing” modes confer to these solution a particular interest in the context of DNA studies.

## 3.8 Summary and conclusions

We summarize the results presented in this chapter. In the first part of the chapter, we have developed the multiple scale expansion technique for the case of vectorial lattices. This allows the calculation of an approximate solution of the equations of motion in the form of a wave-packet, whose envelope is determined by a Non Linear Schrödinger equation.

We then apply this technique to the *twist-opening* model we have introduced in Chapter 2, obtaining, for the generic case, a solution whose main contribution is composed by a breather in the radial component of the field and a kink distortion in angles, which depends on the integral over the whole radial displacement. The angular kink corresponds to a local untwist which moves together with the radial breather. The shape of the solution we found is thus in agreement with the structural properties of DNA according to which a local opening must be coupled with a corresponding untwist.

The breather+kink solutions we calculate exist if for the parameters  $P$  and  $Q$  of the NLS equation the relation  $PQ > 0$  holds. This depends on the choice of the wave number  $q$  and of the frequency branch for the central wave-packet mode of oscillation, as well as on the model parameters. In the second part of the chapter, therefore, we discuss which solutions are admitted for different parameter choices. We focus on solutions with small wave number  $q$ , because their features are similar to the bubble like distortions we consider in DNA.

The study of the existence range for the breather+kink solution show that, with the present choice of constants, the *twist-opening* model, at small  $q$ , admits only “acoustic” solutions, *i.e.* solutions built on an acoustic mode  $(q, \omega_-(q))$ . These solutions are characterized by a large period of oscillation which is not in agreement with experimental data on the DNA “breathing”. We show “optical” solutions with approximately the right frequency, obtained with a different choice of the parameters which is anyway not justified on the basis of experimental data. Therefore, we discuss if it is possible to improve the model in order to recover good solutions.

We suggest that the model, as it is presented in Chapter 2, lacks a specific term which represents the direct stacking interaction due to the overlap of the  $\pi$  electrons of adjacent base pairs. We introduce then the new term,  $W_{stack}$ , into the Lagrangian. With this additional stacking term, our model possesses breather+kink “optical” solutions, shown in the last part of the chapter. The obtained solution has the desired properties and is well stable.

Anyway, the correction we introduce to the stacking implies the addition of one more constant to the set of parameters. We have not yet fixed the parameters of the model in its final form. This will be done in future works.

We have concluded at this point the central part of the work: the building of a DNA model which allows to reproduce some of its dynamical features by taking

into account its geometrical structure and the related constraints. We show that, as one has to expect, localized opening oscillations have to be coupled with a corresponding untwist of the double helix, and that the *twist-opening* model is able to reproduce this feature. By referring to experimental results on the DNA “breathing” model we have adjusted the model, obtaining a more appropriate stacking interaction, in order to fit the available data.

The model we have obtained can be used in studying several DNA processes involving opening and untwist of the helix. In particular, we designed the model by referring to transcription initiation: it has been suggested that small amplitude breathers could act as precursors of the formation of transcription bubbles, through a trap mechanism holding in the promoter region. Further studies will be devoted to investigate this possibility.

Moreover, once we have obtained a good model, with an appropriate choice of the constants, it will be possible to consider other processes and DNA dynamical features, as the possible existence of other kinds of localized movable solutions, the role of breather+kink or other solutions in the action at a distance which is involved in the mechanisms of transcription activation, the effect of the specific base sequence on the dynamical properties of moving distortions, or the possibility of transitions to a left-handed helix, its interaction with moving distortions and the dynamical features of the interface between the two resulting helical configuration.

All these topics will be discussed in future works. For the moment, we would like to complete our comparison with the PB model, by looking at the model features in condition of constant temperature, *i.e.* by canonical ensemble simulations. This leads to observe what kind of distortions can be generated in a chain by thermal energy localization, due to nonlinearity, and allows to compare the features of the denaturation transition for the model with those of real DNA. We will present the results of such simulations in the next chapter.